

Anelastic reorganisation of fibre-reinforced biological tissues

Original

Anelastic reorganisation of fibre-reinforced biological tissues / DI STEFANO, Salvatore; Carfagna, Melania; Knodel, Markus M.; Hashlamoun, Kotaybah; Federico, Salvatore; Grillo, Alfio. - In: COMPUTING AND VISUALIZATION IN SCIENCE. - ISSN 1432-9360. - (2019), pp. 95-109. [10.1007/s00791-019-00313-1]

Availability:

This version is available at: 11583/2736890 since: 2020-02-22T20:10:23Z

Publisher:

Springer

Published

DOI:10.1007/s00791-019-00313-1

Terms of use:

This article is made available under terms and conditions as specified in the corresponding bibliographic description in the repository

Publisher copyright

Springer postprint/Author's Accepted Manuscript

This version of the article has been accepted for publication, after peer review (when applicable) and is subject to Springer Nature's AM terms of use, but is not the Version of Record and does not reflect post-acceptance improvements, or any corrections. The Version of Record is available online at: <http://dx.doi.org/10.1007/s00791-019-00313-1>

(Article begins on next page)

Anelastic reorganisation of fibre-reinforced biological tissues

Salvatore Di Stefano¹ · Melania Carfagna¹ · Markus M. Knodel² ·
Kotaybah Hashlamoun^{3,4} · Salvatore Federico⁴ · Alfio Grillo¹

Received: date / Accepted: date

Abstract In this work, we contribute to the study of the structural reorganisation of biological tissues in response to mechanical stimuli. We specialise our investigation to a class of hydrated soft tissues, whose internal structure features reinforcing fibres. These are oriented statistically within the tissue, and their pattern of orientation is such that, at each material point, the tissue is anisotropic. From its natural, stress-free state, the tissue can be distorted anelastically into a global reference configuration, and then deformed under the action of external mechanical loads. The anelastic distortions are responsible for changing irreversibly the internal structure of the tissue, which, in the present context, occurs through both the rearrangement of the bonds among the tissue cells and the deformation-driven reorientation of the fibres. The anelastic strains, in addition, are assumed to

model the onset and evolution of microcracks in the tissue, which may be triggered by the mechanical loads applied to the tissue in the case of traumatic events, or diseases. For our purposes, we formulate an anisotropic model of remodelling and we consider a fully isotropic model of structural reorganisation for comparison, with the aim to study if, how, and to what extent the evolution of anelastic distortions is influenced by the tissue's anisotropy.

Keywords Anelastic distortions · Fibre-reinforcement · Biological tissues · Anisotropic media

1 Introduction

Biological tissues tend to adapt themselves to the stimuli to which they are exposed and to the environment in which they are placed [60]. By “stimulus” it is meant here any interaction, or combination of interactions, that yields an evolution of mass, composition, shape, and internal structure of a given tissue. An interaction of this kind can be genetic or epigenetic, physiological or pathological, and may be related to the occurrence of phenomena of various nature, associated with different time and length scales.

In this work, emphasis is put on the evolution of the internal structure of fibre-reinforced soft tissues saturated with an interstitial fluid and exchanging mechanical interactions with it [25]. The fibres consist of collagen and are assumed to be directed according to a spatially inhomogeneous statistical distribution of orientations that makes the tissue anisotropic [42, 4, 30, 23, 18]. The interactions with the fluid are usually accounted for under the hypothesis of validity of Darcy's law [41, 56, 3].

Within the modelling framework outlined above, we address a type of structural reorganisation that may be associated with two types of phenomena. The first one, which is often encountered in the study of cellular aggregates and

This work has been partially financed by the *Politecnico di Torino* [AG, SDS, MC, MMK, KH], the *Fondazione Cassa di Risparmio di Torino* in the context of the funding campaign “*La Ricerca dei Talenti*” (HR Excellence in Research) [AG, SDS, MC, MMK, KH], “*Dipartimento di Eccellenza 2018-2022*” (DISMA), Politecnico di Torino [AG, SDS]; the Natural Sciences and Engineering Research Council of Canada, through the NSERC Discovery Programme [SF], and the Biomedical Engineering Programme of the University of Calgary [KH].

Corresponding author: Alfio Grillo (alfio.grillo@polito.it)

¹ Dept. of Mathematical Sciences (DISMA) “G.L. Lagrange”, “*Dipartimento di Eccellenza 2018-2022*”, Politecnico di Torino, C.so Duca degli Abruzzi 24, 10129, Torino (TO) Italy

Tel.: +39-011-0907531

Fax: +39-011-0907599

E-mail: {salvatore.distefano melania.carfagna alfio.grillo}@polito.it

² Dept. of Mathematics, Chair of Applied Mathematics 1, Friedrich-Alexander-Universität Erlangen-Nürnberg, Cauerstr. 11, 91058 Erlangen, Germany

E-mail: markus.knodel@math.fau.de

³ Graduate Programme in Biomedical Engineering, The University of Calgary, 2500 University Drive NW, Calgary, AB T2N 1N4, Canada

⁴ Dept. of Mechanical and Manufacturing Engineering, The University of Calgary, 2500 University Drive NW, Calgary, AB T2N 1N4, Canada
E-mail: {kwhashla salvatore.federico}@ucalgary.ca

tumour spheroids, occurs through the reorganisation of the extracellular matrix of the considered tissue, and leads to the change of the adhesion properties of the tissue cells [55, 31, 39]. The second phenomenon, studied in the mechanics of bone, consists of the emergence of irreversible strains in conjunction with the formation of micro-cracks in diseased or injured tissues [27]. In spite of the fact that the aforementioned phenomena have different nature, both of them can be described by suitably re-interpreting some fundamental concepts of the theory of Plasticity [46, 51] (further details are given in Section 2.1). More specifically, it is stipulated that both the remodelling of a tissue's extra-cellular matrix and the irreversible strains arising in the case of damaged or overloaded tissues can be expressed in terms of plastic-like distortions. The physical meaning of such distortions can be captured by relating them to the concept of residual stresses, which generally accompany the structural changes of a tissue. Since residual stresses persist even when all the loads applied to the tissue are switched off, even an unloaded configuration, taken as reference for the tissue's evolution, may happen to be in a stressed state. Accordingly, it is possible to identify the plastic distortions with the transformations that bring the tissue from the stressed state associated with the chosen reference configuration to a stress-free state, i.e., a state reached by eliminating all applied loads and relaxing all residual stresses [51] (we recall that a similar definition is given in [58] for the remodelling associated with growth).

Determining physically sound evolution laws for the distortions characterising the structural adaptation of biological tissues is a crucial task, which has been undertaken by several authors (see e.g. [16, 45, 28, 1, 43, 29, 53, 36]). One of the main challenges of mathematical modelling is to predict how the structural evolution of a tissue is modulated by mechanical stress. This issue is particularly relevant when also other phenomena, such as growth [57], mechano-transduction [6], and interactions with other stimuli [44, 48, 10], have to be accounted for. Moreover, since the formulation of models for the structural evolution of tissues allows for a certain freedom, and since a model that is reliable for a certain tissue may be inaccurate for another one, it is difficult to find a unified criterion for determining *a priori* how such models should be constructed. To our knowledge, however, Epstein and Maugin [16] prescribed a series of conditions that should be satisfied in order to formulate acceptable structural evolutions. These rules, in turn, are based on the theory developed, for example, in [15, 50, 14].

With the purpose of seeking for a unified form of the structural evolution laws of biological tissues, we take a phenomenological law of remodelling in isotropic media [31] and, by following the rules put forward in [16], we rephrase it for the case of an anisotropic tissue. To this end, we elaborate the anisotropic hyperelastic model of fibre-reinforced tissues developed in [24, 19, 61], in which the interaction

with an interstitial fluid is considered, and we extend it to the case of nonlinear elastoplastic material behaviour. Then, after specifying the equations governing the deformation of the tissue, the fluid flow, and the evolution of the plastic-like distortions, we test our model by solving numerically dedicated benchmark problems. The main result of our work is the evaluation of the interplay between remodelling and the anisotropy of the tissue. This interplay is highlighted by comparing the results of our anisotropic model with those predicted by an isotropic model taken as reference [39].

2 Theoretical background

We adopt with slight variations the covariant formalism of Continuum Mechanics presented in [47].

The motion of the solid phase is described in terms of a one-parameter family of embeddings $\chi_t : \mathcal{B} \rightarrow \mathcal{S}$, where $t \in \mathcal{I}$ is time and $\mathcal{I} \subseteq \mathbb{R}$ is an interval, \mathcal{S} is the three-dimensional Euclidean space, and the open set $\mathcal{B} \subset \mathcal{S}$ is said to be the reference configuration of the tissue. It holds that $\chi_t(X) = \chi(X, t)$, with $\chi : \mathcal{B} \times \mathcal{I} \rightarrow \mathcal{S}$.

For every $x \in \mathcal{S}$ and $X \in \mathcal{B}$, $T_x\mathcal{S}$ and $T_X\mathcal{B}$ are the tangent spaces of \mathcal{S} and \mathcal{B} at x and X , respectively. The disjoint unions $T\mathcal{S} := \sqcup_{x \in \mathcal{S}} T_x\mathcal{S}$ and $T\mathcal{B} := \sqcup_{X \in \mathcal{B}} T_X\mathcal{B}$ are the tangent bundles of \mathcal{S} and \mathcal{B} . The spaces dual to $T_x\mathcal{S}$ and $T_X\mathcal{B}$ are referred to as co-tangent spaces and denoted by $T_x^*\mathcal{S}$ and $T_X^*\mathcal{B}$, while $T^*\mathcal{S} := \sqcup_{x \in \mathcal{S}} T_x^*\mathcal{S}$ and $T^*\mathcal{B} := \sqcup_{X \in \mathcal{B}} T_X^*\mathcal{B}$ are the co-tangent bundles. Finally, \mathcal{B} and \mathcal{S} are equipped with the metric tensors \mathbf{G} and \mathbf{g} , respectively.

The tangent map of $\chi_t : \mathcal{B} \rightarrow \mathcal{S}$ is the deformation gradient tensor $\mathbf{F}(X, t) : T_X\mathcal{B} \rightarrow T_{\chi_t(X)}\mathcal{S}$. Once two local systems of coordinates are chosen in \mathcal{B} and \mathcal{S} , the components of \mathbf{F} read $F_A^a = \partial\chi^a/\partial X^A \equiv \chi_{,A}^a$, with $a, A = 1, 2, 3$. The determinant $J = \det \mathbf{F}$, called *volumetric ratio*, is required to be strictly positive at all points $X \in \mathcal{B}$ and at all times. Another measure of deformation that will be used in the following is the right Cauchy-Green deformation tensor defined by $\mathbf{C} = \mathbf{F}^T \mathbf{g} \mathbf{F} \equiv \mathbf{F}^T \cdot \mathbf{F}$.

2.1 Anelastic distortions and natural state

As anticipated in Section 1, the structural evolution of a tissue is interpreted as a sequence of plastic-like distortions, described by a *distortion tensor*. This tensor, denoted by \mathbf{F}_p , is introduced by invoking the Bilby-Kröner-Lee (BKL) decomposition of the deformation gradient tensor. Consequently, \mathbf{F} is written as $\mathbf{F} = \mathbf{F}_e \mathbf{F}_p$, where \mathbf{F}_e is said to be the tensor of elastic distortions and $J = J_e J_p$, with $J_e := \det \mathbf{F}_e > 0$ and $J_p := \det \mathbf{F}_p > 0$. In the literature, decompositions of the deformation gradient tensor have been extensively used to address problems of biomechanical interest (see e.g. [58, 16,

45, 1, 2, 26, 36, 39, 40]). The physical and geometrical meaning of the BKL decomposition have been explained in detail, for instance, in [51, 32] and they have been recently used to study the structural evolution of a growing tumour in [10]. For every pair $(X, t) \in \mathcal{B} \times \mathcal{I}$, $\mathbf{F}_p(X, t)$ maps $T_X\mathcal{B}$ into a vector space, denoted by $\mathcal{N}_X(t)$ and consisting in the image of $T_X\mathcal{B}$ through $\mathbf{F}_p(X, t)$ [10], whose vectors represent body elements in a stress-free state [11]. In general, \mathbf{F}_p is an *incompatible* tensor (see [51, 59] and references therein). The way in which $\mathbf{F}_p(X, t)$ operates on $T_X\mathcal{B}$ is illustrated in Figure 1.

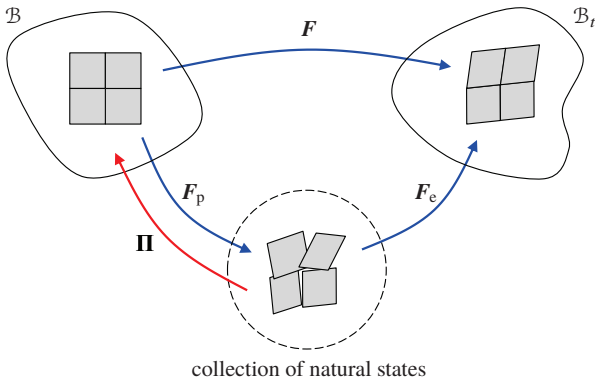


Fig. 1 Multiplicative decomposition of the deformation gradient tensor \mathbf{F} . When the BKL decomposition is enforced, the rule $\mathbf{F} = \mathbf{F}_e\mathbf{F}_p$ applies. When, instead, the decomposition *à la* Epstein and Maugin [15, 50] is employed, the rule $\mathbf{F}\mathbf{\Pi} = \mathbf{F}_e$ is used.

In light of the BKL decomposition, each vector in the natural state $\mathbf{u}_X(t) \in \mathcal{N}_X(t)$ can be distorted elastically into $\mathbf{u}_x(t) = \mathbf{F}_e(X, t)\mathbf{u}_X(t) \in T_x\mathcal{S}$, with $x = \chi_t(X)$. Moreover, we introduce the tensor $\mathbf{\Pi}(X, t) : \mathcal{N}_X(t) \rightarrow T_X\mathcal{B}$ as the inverse of $\mathbf{F}_p(X, t)$, so that the relation $\mathbf{U}_X = \mathbf{\Pi}(X, t)\mathbf{u}_X(t) \in T_X\mathcal{B}$ holds true. Finally, we notice that, since $\mathbf{F}(X, t) : T_X\mathcal{B} \rightarrow T_x\mathcal{S}$ is such that $\mathbf{u}_x(t) = \mathbf{F}(X, t)\mathbf{U}_X$, with $x = \chi_t(X)$, it also holds true that

$$\begin{aligned} \mathbf{u}_x(t) &= \mathbf{F}(X, t)\mathbf{U}_X = \mathbf{F}(X, t)\mathbf{\Pi}(X, t)\mathbf{u}_X(t) \\ &= \mathbf{F}_e(X, t)\mathbf{u}_X(t). \end{aligned} \quad (1)$$

It follows thus from this chain of equalities, which has to be respected for all $\mathbf{u}_X(t) \in \mathcal{N}_X(t)$, that the elastic distortion tensor is given by $\mathbf{F}_e = \mathbf{F}\mathbf{\Pi}$. We remark that this result goes far behind the simple renaming of \mathbf{F}_p^{-1} with $\mathbf{\Pi}$, for it actually discloses the possibility of exploring some analogies of the BKL decomposition with the theory of material uniformity [15, 50, 16, 14, 54] (quoting *verbatim* from [16] “a body is said to be materially uniform if all its points are made of the same material”). However, we do not speculate here on this analogy because it is out of the scope of our work.

2.2 The fibre pattern

Following the framework presented in [24, 19, 61, 5, 34, 35], also in this work we study fibre-reinforced tissues in which the fibres are oriented statistically. The first assumption of our approach is that, at each material point X that finds itself in a natural state, the tissue is transversely isotropic with respect to the direction associated with the unit vector \mathbf{m}_X , which defines the direction of local alignment of the fibre passing through X . The second assumption is that the fibres’ directional distribution is such that the tissue as a whole is transversely isotropic with respect to a global symmetry axis, identified with the unit vector \mathbf{m}_0 . Moreover, in the sequel we restrict our attention to a sample of tissue characterised by cylindrical shape and material properties that vary only along its geometrical axis. The sample is thus homogeneous on each cross section. A consequence of this setting is that the sample’s geometrical axis coincides with the axis of transverse isotropy, which is also then symmetry axis of the tissue.

To account for the statistical orientation of the fibres, we adhere to the framework discussed in [19] and we introduce the function $\wp_X : \mathbb{S}^2\mathcal{N}_X(t) \rightarrow \mathbb{R}_0^+$, with

$$\mathbb{S}^2\mathcal{N}_X(t) := \{\mathbf{m}_X \in \mathcal{N}_X(t) : \|\mathbf{m}_X\| = 1\}, \quad (2)$$

and $\wp_X(\mathbf{m}_X)$ measuring the probability density that a (rectified) fibre passing through X be directed along \mathbf{m}_X .

With respect to an orthonormal vector basis $\{\mathbf{e}_\alpha\}_{\alpha=1}^3$ of $\mathcal{N}_X(t)$, such that \mathbf{e}_3 is parallel to \mathbf{m}_0 , a unit vector $\mathbf{m}_X \in \mathcal{N}_X(t)$ can be expressed in spherical coordinates as $\mathbf{m}_X = \check{\mathbf{m}}_X(\vartheta, \varphi)$, where the vector-valued function $\check{\mathbf{m}}_X : [0, \pi] \times [0, 2\pi[\rightarrow \mathbb{S}^2\mathcal{N}_X(t)$ is given by

$$\check{\mathbf{m}}_X(\vartheta, \varphi) = \sin \vartheta \cos \varphi \mathbf{e}_1 + \sin \vartheta \sin \varphi \mathbf{e}_2 + \cos \vartheta \mathbf{e}_3. \quad (3)$$

Accordingly, a physical quantity \mathfrak{F}_X depending on the local direction of fibre alignment, and thus defined over the set $\mathbb{S}^2\mathcal{N}_X(t)$, can be rewritten as a function of ϑ and φ , i.e., $\mathfrak{F}_X(\mathbf{m}_X) = \mathfrak{F}_X(\check{\mathbf{m}}_X(\vartheta, \varphi)) = \check{\mathfrak{F}}_X(\vartheta, \varphi)$. In particular, the probability density becomes $\wp_X(\mathbf{m}_X) = \check{\wp}_X(\vartheta, \varphi)$ and, since the tissue as a whole is assumed to be transversely isotropic with respect to \mathbf{m}_0 , $\check{\wp}$ is not allowed to depend on the longitude, φ . Consequently, the equality $\wp_X(\mathbf{m}_X) = \check{\wp}_X(\vartheta)$ must be fulfilled.

Following the formalism adopted in [20], the directional average of \mathfrak{F}_X is defined as

$$\begin{aligned} \langle\langle \mathfrak{F}_X(\mathbf{m}_X) \rangle\rangle &= \int_{\mathbb{S}^2\mathcal{N}_X(t)} \mathfrak{F}_X(\mathbf{m}_X) \wp_X(\mathbf{m}_X) \\ &= \int_0^{2\pi} \int_0^\pi \check{\mathfrak{F}}_X(\vartheta, \varphi) \check{\wp}_X(\vartheta) \sin \vartheta d\vartheta d\varphi. \end{aligned} \quad (4)$$

All physical quantities featuring in the mathematical model, including the probability density, are assumed to be invariant

under the reflection $\mathbf{m}_X \mapsto -\mathbf{m}_X$, for all \mathbf{m}_X . This permits to rephrase the directional average (4) as

$$\begin{aligned} \langle \tilde{\gamma}_X(\mathbf{m}_X) \rangle &= 2 \int_{\mathbb{S}^{2+}\mathcal{N}_X(t)} \tilde{\gamma}_X(\mathbf{m}_X) \wp_X(\mathbf{m}_X) \\ &= \int_0^{2\pi} \int_0^{\pi/2} \tilde{\gamma}_X(\vartheta, \varphi) \tilde{\psi}_X(\vartheta) \sin \vartheta d\vartheta d\varphi, \end{aligned} \quad (5)$$

where $\mathbb{S}^{2+}\mathcal{N}_X(t)$ is the “northern” hemisphere [5], i.e.,

$$\mathbb{S}^{2+}\mathcal{N}_X(t) := \{\mathbf{m}_X \in \mathbb{S}^2\mathcal{N}_X(t) : \mathbf{m}_X \cdot \mathbf{m}_0 \geq 0\}, \quad (6)$$

and the probability density $\tilde{\psi}_X : [0, \pi/2] \rightarrow \mathbb{R}_0^+$ is defined by the equality $\tilde{\psi}_X(\vartheta) = \psi_X(\tilde{\mathbf{m}}_X(\vartheta, \varphi))$, for all $(\vartheta, \varphi) \in [0, \pi/2] \times [0, 2\pi]$, with $\psi_X = 2\wp_X|_{\mathbb{S}^{2+}\mathcal{B}}$ [5]. As done in previous works [21, 5], we assume that $\tilde{\psi}_X$ is the pseudo-Gaussian distribution

$$\tilde{\psi}_X(\vartheta) = \frac{\tilde{\gamma}_X(\vartheta)}{2\pi \int_0^{\pi/2} \tilde{\gamma}_X(\vartheta') \sin \vartheta' d\vartheta'}, \quad (7a)$$

$$\tilde{\gamma}_X(\vartheta) = \exp\left(-\frac{[\vartheta - q]^2}{2\omega^2}\right), \quad (7b)$$

where q and ω are referred to as fibre mean angle and standard deviation, respectively. Since, as anticipated above, q and ω are hypothesised to vary only along the axis of the sample, they can be written as functions of the normalised axial variable $\xi \in [0, 1]$, which is zero at the sample’s lower boundary and equal to one at the upper boundary. Hereafter, we prescribe the expressions

$$q(\xi) = \frac{\pi}{2} \left\{ 1 - \cos\left(\frac{\pi}{2} \left[-\frac{2}{3}\xi^2 + \frac{5}{3}\xi\right]\right) \right\}, \quad (8a)$$

$$\omega(\xi) = 10^3[(1 - \xi)\xi]^4 + 3 \cdot 10^{-2}, \quad (8b)$$

which qualitatively reproduce the alignment of fibres in articular cartilage [52]. According to (8a) and (8b), the mean angle takes on the values $q(0) = 0$ and $q(1) = \pi/2$, and the standard deviation attains its minimum at $\xi = 0$ and $\xi = 1$. Hence, the fibres are more likely to be found aligned with the sample’s symmetry axis at the bottom of the sample, and more likely to be lying on transverse plane at the top. Moreover, at $\xi = 1/2$, the standard deviation reaches its maximum, thereby tending to randomise the fibre orientation and, consequently, to make the tissue isotropic in the middle of the sample.

Note that $\mathbf{m} : \mathcal{B} \rightarrow \mathcal{N}(t)$ indicates the vector field such that $\mathbf{m}(X) = \mathbf{m}_X$, and $\mathcal{N}(t) := \sqcup_{X \in \mathcal{B}} \mathcal{N}_X(t)$ is the bundle of all spaces $\mathcal{N}_X(t)$.

2.3 Constitutive laws

At each material point, the solid phase of the tissue is modelled as a hyperelastic material. This hypothesis allows to describe the mechanical behaviour of the solid phase entirely in terms of a strain energy density, and to express the latter as a function of the elastic part of the deformation, only. More precisely, if $W_R = \hat{W}_R(\mathbf{C}, X, t)$ denotes the strain energy density of the solid phase, written per unit volume of the reference configuration (note that the the material inhomogeneities and their evolution are accounted for by the explicit dependence of \hat{W}_R on the material points and time, respectively), it is possible to write [7, 16]

$$\hat{W}_R(\mathbf{C}, X, t) = \frac{1}{J_{\Pi}(X, t)} \hat{W}_v(\mathbf{C}_e(X, t), X), \quad (9)$$

where \hat{W}_v is measured per unit volume of the natural state, $J_{\Pi} = \det \Pi$ and $\mathbf{C}_e = \mathbf{F}_e^T \cdot \mathbf{F}_e = \mathbf{F}_e^T \mathbf{g} \mathbf{F}_e = \Pi^T \mathbf{C} \Pi$ is the *elastic part of the right Cauchy-Green deformation tensor*. We remark that, in Equation (9), the explicit dependence of the strain energy function on material points is given through ξ . In the following, however, for the sake of a lighter notation, the explicit dependence of \hat{W}_v on material points, X , is omitted but understood, and we adapt to the present framework a strain energy density used in previous works [24, 19, 61, 5, 40, 35], i.e.,

$$\hat{W}_v(\mathbf{C}_e) = \Phi_{sv} \hat{U}(J_e) + \Phi_{0sv} \hat{W}_0(\mathbf{C}_e) + \Phi_{1sv} \hat{W}_{en}(\mathbf{C}_e), \quad (10)$$

where

$$\Phi_{0sv} = J_e \phi_{0s}, \quad (11a)$$

$$\Phi_{1sv} = J_e \phi_{1s}, \quad (11b)$$

$$\Phi_{sv} = \Phi_{0sv} + \Phi_{1sv} = J_e \phi_s \quad (11c)$$

are the volumetric fractions of the non-fibrous matrix, fibres, and solid phase as a whole, respectively, all measured per unit volume of the natural state, while $\hat{U}(J_e)$, $\hat{W}_0(\mathbf{C}_e)$, and $\hat{W}_{en}(\mathbf{C}_e)$ are given by

$$\hat{U}(J_e) = \alpha_0 \mathcal{H}(J_{cr} - J_e) \frac{[J_e - J_{cr}]^{2q}}{[J_e - \Phi_{sv}]^r}, \quad (12a)$$

$$\hat{W}_0(\mathbf{C}_e) = \alpha_0 \left[\frac{\exp(\alpha_1 [I_{1e} - 3] + \alpha_2 [I_{2e} - 3])}{[I_{3e}]^{\alpha_3}} - 1 \right], \quad (12b)$$

$$\hat{W}_{en}(\mathbf{C}_e) = \hat{W}_{li}(\mathbf{C}_e) + \langle \hat{W}_{1a}(\mathbf{C}_e, \mathbf{m}) \rangle. \quad (12c)$$

In (12a)–(12c), $\alpha_0 = 0.125$ MPa, $\alpha_1 = 0.778$, $\alpha_2 = 0.111$, $\alpha_3 = \alpha_1 + 2\alpha_2 = 1$, $q \geq 0$, and $r \in [0, 1]$ are material parameters, $J_{cr} \in [\Phi_{sv}, 1]$ is a critical value of J_e (in this work, we take $q = 2$, $r = 0.5$, and $J_{cr} = \Phi_{sv} + 0.1$), $I_{1e} = \text{tr}(\mathbf{C}_e)$, $I_{2e} = \frac{1}{2}\{\text{tr}(\mathbf{C}_e)^2 - \text{tr}(\mathbf{C}_e^2)\}$, and $I_{3e} = \det \mathbf{C}_e$ are the principal invariants of \mathbf{C}_e , \hat{W}_{li} is the isotropic part of the strain energy density of the fibres (it has the same functional form as (12b), but it features different coefficients), and $\hat{W}_{1a}(\mathbf{C}_e, \mathbf{m})$ reads

$$\hat{W}_{1a}(\mathbf{C}_e, \mathbf{m}) = \mathcal{H}(I_{4e} - 1) \frac{1}{2} c [I_{4e} - 1]^2, \quad (13)$$

where $I_{4e} = \mathbf{C}_e : \mathbf{m} \otimes \mathbf{m} = \mathbf{C} : (\mathbf{\Pi} \mathbf{m} \otimes \mathbf{\Pi} \mathbf{m})$ and $c = 7.46$ MPa. In (12a) and (13), \mathcal{H} is the Heaviside function, i.e., $\mathcal{H}(s) = 1$ for all $s \geq 1$, and $\mathcal{H}(s) = 0$ for all $s < 0$. Finally, it is possible to define the unit vector field

$$\mathbf{M} = \frac{\mathbf{\Pi} \mathbf{m}}{\|\mathbf{\Pi} \mathbf{m}\|}. \quad (14)$$

Consequently, the structure tensor field associated with the natural state, i.e., $\mathbf{a} = \mathbf{m} \otimes \mathbf{m}$, transforms as

$$\mathbf{A} = \mathbf{M} \otimes \mathbf{M} = \frac{\mathbf{\Pi} \mathbf{a} \mathbf{\Pi}^T}{(\mathbf{\Pi}^T \cdot \mathbf{\Pi}) : \mathbf{a}}, \quad (15)$$

with \mathbf{A} being the structure tensor field associated with the reference configuration, and the invariant I_{4e} becomes $I_{4e} = I_4 I_{4\Pi}$, where we used the notation

$$I_4 = \mathbf{C} : \mathbf{A}, \quad (16a)$$

$$I_{4\Pi} = (\mathbf{\Pi}^T \cdot \mathbf{\Pi}) : \mathbf{a}. \quad (16b)$$

The energy $\hat{U}(J_e)$ is zero for J_e above the critical volume ratio J_{cr} (which, in general, is a function of material points), and diverges for J_e tending to Φ_{sv} from above, thereby preventing the elastic distortions from violating the unilateral constraint $J_e \geq \Phi_{sv}$. The constitutive part of the first Piola-Kirchhoff stress tensor associated with the solid phase is given by

$$\mathbf{P} = \mathbf{F} \left[\frac{1}{J_{\Pi}} \mathbf{\Pi} \left(2 \frac{\partial \hat{W}_v}{\partial \mathbf{C}_e}(\mathbf{C}_e) \right) \mathbf{\Pi}^T \right]. \quad (17)$$

Consequently, \mathbf{P} can be expressed constitutively as a function of \mathbf{F} and $\mathbf{\Pi}$, i.e., $\mathbf{P} = \hat{\mathbf{P}}(\mathbf{F}, \mathbf{\Pi})$. Also in this case, the explicit dependence on material points is omitted but understood.

The system under study, comprising a porous solid phase (i.e., matrix and reinforcing fibres) and an interstitial fluid, is assumed to be saturated, thereby meaning that the porosity of the medium coincides with the volumetric fraction of the fluid, which is thus given by $\phi_f = 1 - \phi_s$.

The mathematical model presented in the following is based on the hypothesis that the interstitial fluid obeys Darcy's law. This requires the introduction of a permeability tensor for the tissue. In this work, we adapt to our problem the constitutive framework developed in [23, 22, 19, 61, 34]. Hence, we assume that the spatial permeability tensor reads [61]

$$\mathbf{k} = k_0 \frac{[JJ_{\Pi} - \Phi_{1sv}]^2}{J^2 J_{\Pi}^2} \mathbf{g}^{-1} + k_0 \frac{[JJ_{\Pi} - \Phi_{1sv}]\Phi_{1sv}}{J^2 J_{\Pi}^2} \mathbf{F} \mathbf{\Pi} \left\langle \frac{\mathbf{a}}{I_{4e}} \right\rangle \mathbf{\Pi}^T \mathbf{F}^T, \quad (18)$$

where k_0 is taken to be of the Holmes&Mow type [41], i.e.,

$$k_0 = k_{0v} \left[\frac{JJ_{\Pi} - \Phi_{sv}}{1 - \Phi_{sv}} \right]^{\kappa_0} \exp \left(\frac{1}{2} m_0 [J^2 J_{\Pi}^2 - 1] \right), \quad (19)$$

where $\kappa_0 = 0.0848$ and $m_0 = 4.638$ are model parameters, and k_{0v} is a reference permeability. As done elsewhere (e.g.

in [61]), k_{0v} is taken as a function of the axial coordinate, ξ , and its functional form is defined in (22). From (18) and (19) we notice that, since the product $JJ_{\Pi} = J_e$ has to be greater than, or equal to, Φ_{sv} , the permeability tensor is positive semi-definite for $JJ_{\Pi} \geq \Phi_{sv} \geq \Phi_{1sv}$ and, in particular, it is positive definite when the strict inequality is satisfied, i.e., when $JJ_{\Pi} > \Phi_{sv}$.

For future use, we compute the Piola transform of \mathbf{k} , i.e., $\mathbf{K} = J\mathbf{F}^{-1} \mathbf{k} \mathbf{F}^{-T}$, which reads

$$\mathbf{K} = k_0 \frac{[JJ_{\Pi} - \Phi_{1sv}]^2}{JJ_{\Pi}^2} \mathbf{C}^{-1} + k_0 \frac{[JJ_{\Pi} - \Phi_{1sv}]\Phi_{1sv}}{JJ_{\Pi}^2} \mathbf{\Pi} \left\langle \frac{\mathbf{a}}{I_{4e}} \right\rangle \mathbf{\Pi}^T. \quad (20)$$

Clearly, since \mathbf{k} is positive semi-definite, \mathbf{K} is positive semi-definite too. Note also that \mathbf{K} can be written as $\mathbf{K} = \hat{\mathbf{K}}(\mathbf{F}, \mathbf{\Pi})$, where the dependence on \mathbf{F} is through \mathbf{C} because of objectivity, and the dependence on $\mathbf{\Pi}$ is understood. In fact, in the case of inhomogeneous materials, the dependence of k_{0v} on material points can be taken into account by expressing k_{0v} as a function of the void ratio associated with the natural state, $e_v = (1 - \Phi_{sv})/\Phi_{sv}$, and specifying how the volumetric fraction Φ_{sv} depends on the normalised axial coordinate ξ (we recall, indeed, that the material is assumed here to be inhomogeneous only axially). In this work, we assign the volumetric fractions of matrix and fibres in the tissue's natural state, Φ_{0sv} and Φ_{1sv} , and we compute thus the volumetric fraction of the solid phase as $\Phi_{sv} = \Phi_{0sv} + \Phi_{1sv}$. In particular, we prescribe [61]

$$\Phi_{0sv} = \hat{\Phi}_{0sv}(\xi) = -0.062\xi^2 + 0.038\xi + 0.046, \quad (21a)$$

$$\Phi_{1sv} = \hat{\Phi}_{1sv}(\xi) = +0.062\xi^2 - 0.138\xi + 0.204, \quad (21b)$$

$$\Phi_{sv} = \hat{\Phi}_{sv}(\xi) = -0.100\xi + 0.250. \quad (21c)$$

Following the constitutive framework adopted in previous works, we assume that k_{0v} depends on e_v as suggested by Holmes&Mow [41]. Hence, given the constant referential void ratio $e_v^{(0)} = 4$ and the constant referential scalar permeability $k_{0v}^{(0)} = 3.7729 \cdot 10^{-3} \text{ mm}^4(\text{Ns})^{-1}$, we assign k_{0v} through the expression [61]

$$\frac{k_{0v}}{k_{0v}^{(0)}} = \left[\frac{e_v}{e_v^{(0)}} \right]^{\kappa_0} \exp \left(\frac{m_0}{2} \left[\left(\frac{1 + e_v}{1 + e_v^{(0)}} \right)^2 - 1 \right] \right). \quad (22)$$

In summary, the constitutive framework adopted in this work describes a hydrated, fibre-reinforced tissue, whose solid phase is hyperelastic, transversely isotropic with respect to a global symmetry axis (the direction of which is identified by the unit vector \mathbf{m}_0), and inhomogeneous along this axis. We emphasise that, within the employed approach, the inhomogeneity is due to the fact that the volumetric fractions of matrix and fibres, Φ_{0sv} and Φ_{1sv} , the standard deviation of

the probability density, ω , and the mean angle of fibre orientation, q , depend on the normalised axial coordinate through the expressions (8a) and (8b), which are in qualitative agreement with the histological features of articular cartilage, as revealed by X-ray diffraction experiments [52].

3 Description of Remodelling

The mathematical model of the physical system under study is characterised by two dissipative phenomena. First we consider the one related to the fluid flow, which is affected by dissipative forces exchanged between the fluid and the solid phase. We prescribe that these forces depend linearly on the filtration velocity $\mathbf{q} = \phi_f[\mathbf{v}_f - \mathbf{v}_s]$ and, by disregarding the influence of gravity on the flow, we obtain Darcy's law, which reads $\mathbf{q} = -\mathbf{k} \text{grad } p$ in spatial form [3], and $\mathbf{Q} = -\mathbf{K} \text{Grad } p$ in the so-called "material" form. Here, $\mathbf{Q} := J\mathbf{F}^{-1}\mathbf{q}$ is the Piola transform of the filtration velocity, and $\text{Grad } p = \mathbf{F}^T \text{grad } p$ is the "material" pressure gradient, obtained by differentiating p with respect to the coordinates associated with the reference configuration. We remark that the filtration velocity represents the specific mass flux vector associated with the motion of the fluid relative to the solid.

The second dissipative phenomenon addressed in this work is due to the reorganisation of the tissue's internal structure. This process is described here in analogy with the theory of finite strain plasticity through $\mathbf{\Pi}$ [16]. The rate with which the anelastic distortions associated with $\mathbf{\Pi}$ evolve in time is given by $\dot{\mathbf{\Lambda}} = \dot{\mathbf{\Pi}}\mathbf{\Pi}^{-1}$ and it will be referred to as *tensor of rate of remodelling*. In the sequel, we shall assume that remodelling is a volume-preserving process, which yields the restriction $J_{\mathbf{\Pi}} = 1$ and implies that $\mathbf{\Lambda}$ is a deviatoric second-order tensor. Within this framework, the generalised force power-conjugate to $\mathbf{\Lambda}$ is the Mandel stress tensor $\mathbf{\Sigma} = \mathbf{C}\mathbf{S}$ [15,50], where $\mathbf{S} = \mathbf{F}^{-1}\mathbf{P}$ is the constitutive part of the second Piola-Kirchhoff stress tensor of the solid phase.

3.1 Dissipation Inequality

By accounting for the contributions due to the flow and remodelling, denoted by $\mathfrak{D}_{\text{flow}}$ and $\mathfrak{D}_{\text{rem}}$, respectively, the dissipation of the system under study can be written as [39]

$$\mathfrak{D}_R = \underbrace{\mathbf{K} : [\text{Grad } p \otimes \text{Grad } p]}_{\mathfrak{D}_{\text{flow}} \geq 0} - \underbrace{\mathbf{\Sigma} : \mathbf{\Lambda}}_{\mathfrak{D}_{\text{rem}}} \geq 0. \quad (23)$$

Since the positive semi-definiteness of \mathbf{K} guarantees that $\mathfrak{D}_{\text{flow}}$ is non-negative for all pressure gradients, the fulfilment of the inequality $\mathfrak{D}_R \geq 0$ is equivalent to requiring the condition $\mathfrak{D}_{\text{rem}} = -\mathbf{\Sigma} : \mathbf{\Lambda} \geq 0$ for all $\mathbf{\Sigma}$ and $\mathbf{\Lambda}$. Moreover, the physical observation that remodelling is triggered by stress

suggests to relate $\mathbf{\Sigma}$ to $\mathbf{\Lambda}$ in such a way that the aforementioned restriction is respected. This should be done, however, by exploiting the fact that $\mathbf{\Sigma}$ complies, by construction, with the symmetry condition $\mathbf{\Sigma}\mathbf{C} = \mathbf{C}\mathbf{S}\mathbf{C} = (\mathbf{\Sigma}\mathbf{C})^T$ [15,50]. Upon setting $\mathbf{Y} := \mathbf{C}\mathbf{S}\mathbf{C}$, this yields the chain of equalities

$$\mathbf{\Sigma} : \mathbf{\Lambda} = (\mathbf{C}\mathbf{S}\mathbf{C}) : (\mathbf{\Lambda}\mathbf{C}^{-1}) = \mathbf{Y} : \text{sym}(\mathbf{\Lambda}\mathbf{C}^{-1}), \quad (24)$$

which allows to rephrase $\mathfrak{D}_{\text{rem}}$ as [15]

$$\mathfrak{D}_{\text{rem}} = -\mathbf{Y} : \text{sym}(\mathbf{\Lambda}\mathbf{C}^{-1}) \geq 0. \quad (25)$$

We recall that the stress tensor \mathbf{Y} can be obtained by expressing the strain energy density as a function of the Piola strain $\mathcal{E} = \frac{1}{2}[\mathbf{G}^{-1} - \mathbf{C}^{-1}]$ [15,50].

We prescribe here that \mathbf{Y} and $\text{sym}(\mathbf{\Lambda}\mathbf{C}^{-1})$ are related to each other through an expression of the type

$$\text{sym}(\mathbf{\Lambda}\mathbf{C}^{-1}) = -\mathcal{R}, \quad (26)$$

where \mathcal{R} is a tensor-valued function that has to be specified constitutively. Equation (26) shall also be referred to as the *remodelling law*.

To satisfy the condition $\mathfrak{D}_{\text{rem}} \geq 0$, we assume here that \mathcal{R} can be written as $\mathcal{R} = \mathbb{T} : \mathbf{Y}$, where \mathbb{T} is a fourth-order tensor endowed with the major symmetry and such that the inequality $\mathfrak{D}_{\text{rem}} = \mathbf{Y} : \mathbb{T} : \mathbf{Y} \geq 0$ is respected for all \mathbf{Y} (i.e., \mathbb{T} has to be positive semi-definite). The constitutive expression defining \mathbb{T} specifies the law of remodelling that one is interested in. It should be noticed, however, that since $\mathbf{\Lambda}$ is deviatoric (i.e., $\text{tr}\mathbf{\Lambda} = 0$), the right-hand-side of (26), \mathcal{R} , must comply with the restriction $\text{tr}(\mathbf{C}\mathcal{R}) = 0$. This requires \mathbb{T} to fulfil the condition $\text{tr}[\mathbf{C}(\mathbb{T} : \mathbf{Y})] = \mathbf{C} : \mathbb{T} : \mathbf{Y} = 0$, for all \mathbf{Y} .

3.2 Remodelling laws

Equation (26) is the remodelling equation and it describes how the anelastic phenomena evolve during all the deformative process. It is formulated as an evolution law for $\mathbf{\Pi}$ through the tensor $\mathbf{\Lambda} = \dot{\mathbf{\Pi}}\mathbf{\Pi}^{-1}$.

In this work, we assume that remodelling occurs at a given material point when the Frobenius norm $\|\text{dev}\boldsymbol{\sigma}\| = \sqrt{g_{ab}[\text{dev}\boldsymbol{\sigma}]^{ac}g_{cd}[\text{dev}\boldsymbol{\sigma}]^{db}}$ of the deviatoric part of the constitutive solid phase Cauchy stress, $\boldsymbol{\sigma} = J^{-1}\mathbf{P}\mathbf{F}^T$, exceeds at that point a threshold equivalent stress, σ_Y , termed "yield stress" in analogy with Plasticity. To take this requirement into account, we write \mathbb{T} as $\mathbb{T} = \zeta\mathbb{L}$, where ζ is a scalar stress-dependent "remodelling switch". Hence, following [31], we prescribe a Perzyna-like model [51]

$$\zeta = \lambda(\phi_s) \left[\frac{\|\text{dev}\boldsymbol{\sigma}\| - \sqrt{2/3}\sigma_Y}{\|\text{dev}\boldsymbol{\sigma}\|} \right]_+, \quad (27)$$

where $\lambda(\phi_s)$ is a material parameter depending on the volumetric fraction of the solid phase, and the operator $[\cdot]_+$ extracts the positive part of the function to which it is applied (see also [8]). In this work, we assume that the yield stress is constant, and we set $\sigma_Y = 0.002$ MPa. We emphasise that $\lambda(\phi_s)$ vanishes for vanishing ϕ_s , since no remodelling may occur if the solid phase is absent. In the following, we adopt the simple law $\lambda(\phi_s) = \lambda_0 \phi_s^2 = \lambda_0 [\Phi_{sv}/J J_\Pi]^2$, with $\lambda_0 = 0.5$ (MPa · s)⁻¹. We also remark that, since the condition $J_\Pi = 1$ applies in this context, the equality $\phi_s = \Phi_{sv}/J$ allows to rephrase the dependence of λ on ϕ_s in terms of the volume ratio J alone, rather than in terms of J and J_Π .

To complete the description of remodelling, it is necessary to specify the fourth-order tensor \mathbb{L} . In this work, we consider the expression

$$\mathbb{L} = \mathbb{M}^* : \mathbb{D} : \mathbb{M}^{*T}, \quad (28)$$

where \mathbb{M}^* and \mathbb{M}^{*T} are specified in Appendix A. The fourth-order tensor \mathbb{D} encodes information about the material properties of the tissue and, in general, is a function of \mathbf{C} and $\mathbf{\Pi}$. With the notation introduced in Appendix A, \mathbb{D} transforms tensors of $([TB]_2^0, \text{sym})$ into tensors of $([TB]_0^2, \text{sym})$. According to (28), the tensor \mathcal{R} featuring in (26) reads

$$\mathcal{R} = \mathbb{T} : \mathbf{Y} = \zeta \mathbb{L} : \mathbf{Y} = \zeta \mathbb{M}^* : \mathbb{D} : \mathbb{M}^{*T} : \mathbf{Y}. \quad (29)$$

We remark that the double-contraction of \mathbb{M}^{*T} with \mathbf{Y} extracts the deviatoric part of \mathbf{Y} with respect to the metric \mathbf{C} , i.e.,

$$\mathbb{M}^{*T} : \mathbf{Y} = \mathbf{Y} - \frac{1}{3} \text{tr}(\mathbf{C}^{-1} \mathbf{Y}) \mathbf{C}. \quad (30)$$

Moreover, by introducing the tensor $\mathbf{Z} := \mathbb{D} : \mathbb{M}^{*T} : \mathbf{Y}$, the left-multiplication by \mathbb{M}^* in (29) leads to

$$\mathcal{R} = \zeta \mathbb{M}^* : \mathbf{Z} = \zeta \left[\mathbf{Z} - \frac{1}{3} \text{tr}(\mathbf{C} \mathbf{Z}) \mathbf{C}^{-1} \right], \quad (31)$$

which guarantees the compliance with the constraint

$$\begin{aligned} 0 &= \text{tr} \mathbf{A} = \text{tr} [\mathbf{C} \text{sym}(\mathbf{A} \mathbf{C}^{-1})] \\ &= -\text{tr}(\mathbf{C} \mathcal{R}) = -\zeta \text{tr}[\mathbf{C}(\mathbb{M}^* : \mathbf{Z})] = 0. \end{aligned} \quad (32)$$

For the sake of simplicity, in the following we set $\mathbb{D} = \mathbb{I}^{\#*}$ (see Appendix A for the definition of $\mathbb{I}^{\#*}$), which implies

$$\begin{aligned} \mathbf{Z} &= \mathbb{I}^{\#*} : \mathbb{M}^{*T} : \mathbf{Y} \\ &= \mathbf{S} - \frac{1}{3} \text{tr}(\mathbf{C} \mathbf{S}) \mathbf{C}^{-1} = \mathbb{M}^* : \mathbf{S} = \tilde{\mathbf{S}}, \end{aligned} \quad (33a)$$

$$\begin{aligned} \mathbb{L} : \mathbf{Y} &= \mathbb{M}^* : \mathbf{Z} = \mathbb{M}^* : \mathbb{I}^{\#*} : \mathbb{M}^{*T} : \mathbf{Y} \\ &= \mathbb{M}^{\#*} : \mathbf{Y}, \end{aligned} \quad (33b)$$

where $\tilde{\mathbf{S}}$ is said to be the deviatoric part of \mathbf{S} with respect to the metric \mathbf{C} , and $\mathbb{M}^{\#*}$ is defined in Appendix A. Furthermore, since \mathbb{M}^* is idempotent (i.e., it holds that $\mathbb{M}^* : \mathbb{M}^* = \mathbb{M}^*$), we obtain the identity

$$\mathbb{M}^* : \mathbf{Z} = \mathbb{M}^* : \mathbb{M}^* : \mathbf{S} = \mathbb{M}^* : \mathbf{S} = \mathbf{Z}. \quad (34)$$

Thus, Equation (31) reduces to

$$\mathcal{R} = \zeta \mathbb{M}^* : \mathbf{Z} = \zeta \mathbf{Z} = \zeta \left[\mathbf{S} - \frac{1}{3} \text{tr}(\mathbf{C} \mathbf{S}) \mathbf{C}^{-1} \right], \quad (35)$$

and the remodelling law takes on the form

$$\text{sym}(\mathbf{A} \mathbf{C}^{-1}) = -\zeta \left[\mathbf{S} - \frac{1}{3} \text{tr}(\mathbf{C} \mathbf{S}) \mathbf{C}^{-1} \right] = -\zeta \tilde{\mathbf{S}}, \quad (36)$$

thereby satisfying the requirement (32).

3.2.1 Model M1: Fully isotropic model

We use this model for comparison with the other ones, and we obtain it in the limit of vanishing volumetric fraction of the fibres. Hence, we set $\Phi_{1sv} = 0$, which implies $\Phi_{0sv} = \Phi_{sv}$, and we rewrite the strain energy density (10) as

$$\hat{W}_v(\mathbf{C}_e) = \Phi_{sv} \hat{U}(J_e) + \Phi_{sv} \hat{W}_0(\mathbf{C}_e). \quad (37)$$

Consequently, the second Piola-Kirchhoff stress tensor consists of the isotropic contribution only, i.e.,

$$\mathbf{S}_{\text{iso}} = \frac{1}{J_\Pi} \mathbf{\Pi} \left[2\Phi_{sv} \left(\frac{\partial \hat{U}}{\partial C_e} + \frac{\partial \hat{W}_0}{\partial C_e} \right) \right] \mathbf{\Pi}^T, \quad (38)$$

and the permeability tensor reduces to $\mathbf{K}_{\text{iso}} = J k_0 \mathbf{C}^{-1}$. Furthermore, we prescribe the remodelling law

$$\text{sym}(\mathbf{A} \mathbf{C}^{-1}) = -\mathcal{R}_{(1)} = -\zeta \mathbb{L} : \mathbf{Y}_{\text{iso}}. \quad (39)$$

with $\mathbf{Y}_{\text{iso}} = \mathbf{C} \mathbf{S}_{\text{iso}} \mathbf{C}$. By substituting \mathbf{Y}_{iso} into (39) and performing all the necessary algebraic calculations, we obtain

$$\text{sym}(\mathbf{A} \mathbf{C}^{-1}) = -\mathcal{R}_{(1)} = -\zeta \tilde{\mathbf{S}}_{\text{iso}}, \quad (40)$$

$$\text{with } \tilde{\mathbf{S}}_{\text{iso}} = \mathbb{M}^* : \mathbf{S}_{\text{iso}} = \mathbf{S}_{\text{iso}} - \frac{1}{3} \text{tr}(\mathbf{C} \mathbf{S}_{\text{iso}}) \mathbf{C}^{-1}.$$

3.2.2 Model M2: Semi-isotropic model

In this model, we use the full permeability tensor defined in (20) and the transversely isotropic strain energy density (10), which produces the second Piola-Kirchhoff stress tensor

$$\mathbf{S} = \mathbf{S}_i + \mathbf{S}_a, \quad (41)$$

with

$$\mathbf{S}_i = \frac{1}{J_\Pi} \mathbf{\Pi} \left[2\Phi_{sv} \frac{\partial \hat{U}}{\partial C_e} + 2\Phi_{0sv} \frac{\partial \hat{W}_0}{\partial C_e} + 2\Phi_{1sv} \frac{\partial \hat{W}_{1i}}{\partial C_e} \right] \mathbf{\Pi}^T, \quad (42a)$$

$$\mathbf{S}_a = \frac{1}{J_\Pi} \mathbf{\Pi} \left[2\Phi_{1sv} \frac{\partial \langle \hat{W}_{1a} \rangle}{\partial C_e} \right] \mathbf{\Pi}^T. \quad (42b)$$

Note that \mathbf{S}_i and \mathbf{S}_a represent, respectively, the isotropic and transversely isotropic contributions to the overall constitutive part of the second Piola-Kirchhoff stress tensor of the solid phase, \mathbf{S} .

In spite of the fact that both the elastic and the hydraulic response of the tissue are transversely isotropic, we consider the same remodelling law as in the Model M1. Hence, we set

$$\text{sym}(\Lambda C^{-1}) = -\mathcal{R}_{(2)} = -\zeta \mathbb{L} : Y, \quad (43)$$

where Y splits additively as $Y = CSC = CS_i C + CS_a C$. Analogously to the Model M1, also in this case the remodelling law can be written as

$$\text{sym}(\Lambda C^{-1}) = -\mathcal{R}_{(2)} = -\zeta [\tilde{S}_i + \tilde{S}_a], \quad (44)$$

with

$$\tilde{S}_i = \mathbb{M}^* : S_i = S_i - \frac{1}{3} \text{tr}(CS_i) C^{-1}, \quad (45a)$$

$$\tilde{S}_a = \mathbb{M}^* : S_a = S_a - \frac{1}{3} \text{tr}(CS_a) C^{-1} \quad (45b)$$

being the deviatoric parts of S_i and S_a , respectively, with respect to the deformed metric C . We remark that, according to (44), the presence of the fibres supplies a direct contribution to the remodelling law through \tilde{S}_a .

Remark Each remodelling law, i.e., (39) or (43), is in general equivalent to a set of six scalar differential equations in the components of Π . However, when the isochoric condition $J_\Pi = 1$ is enforced, as is the case in this work, the number of independent equations is five, because the constraint $\text{tr}(\Lambda) = \text{tr}(\dot{\Pi}\Pi^{-1}) = 0$ has to be respected. Since, in general, Π possesses nine independent components, which become eight when the isochoric condition $J_\Pi = 1$ applies, the remodelling laws are not closed. To obtain the closure, we perform the polar decomposition of Π , i.e., $\Pi = V \cdot R \equiv VGR$, where R is a rotation tensor and V is a symmetric and positive-definite tensor. In this work, we impose that the rotations associated with remodelling are not allowed, so that only V is unknown. Since it has only six independent components (actually five, because it holds that $J_\Pi = \det V = 1$), the remodelling laws become closed. We also notice that the identity $\Lambda = \dot{\Pi}\Pi^{-1} = \dot{V}V^{-1}$ holds true.

4 Benchmark test and numerical settings

We formulate a finite strain poroplastic problem for a porous medium in which the interstitial fluid obeys Darcy's law and the solid phase exhibits hyperelastic behaviour. Given the reference configuration of the tissue $\mathcal{B} \subset \mathcal{S}$ and the interval of time $I \subset \mathbb{R}$, find the motion χ , pressure p , and V such that

$$\text{Div}(K \text{Grad } p) = \dot{J}, \quad \text{in } \mathcal{B} \times I, \quad (46a)$$

$$\text{Div}(-Jp g^{-1} F^{-T} + P) = 0, \quad \text{in } \mathcal{B} \times I, \quad (46b)$$

$$\text{sym}(\Lambda C^{-1}) = -\mathcal{R}, \quad \text{in } \mathcal{B} \times I, \quad (46c)$$

where \mathcal{R} can be equal to $\mathcal{R}_{(1)}$ or $\mathcal{R}_{(2)}$, depending on whether the model M1 or M2 is computed. We emphasise that, by construction, both $\mathcal{R}_{(1)}$ and $\mathcal{R}_{(2)}$ have to be understood as functionals of χ , and V , i.e., $\mathcal{R}_{(\alpha)} = \hat{\mathcal{R}}_{(\alpha)}(\chi, V)$, for $\alpha \in \{1, 2\}$. Whereas (46c) expresses the general form of the investigated remodelling law, (46a) and (46b) represent, respectively, the mass balance law and the momentum balance law for the biphasic system with which the tissue is approximated. We recall, indeed, that the tissue is assumed here to consist of a solid phase, which comprises a porous matrix and the reinforcing fibres, and an inviscid interstitial fluid obeying Darcy's law. Equations (46a)–(46c) are determined under the hypotheses that the mass densities of the solid and the fluid phase are constant (a condition implying the intrinsic incompressibility of both phases), and that all the external body forces—including the inertial ones—as well as all the quantities of order higher than the first in the relative velocity $v_{fs} := v_f - v_s$ are negligible. More specifically, the mass balance law (46a) implies that the opposite of the divergence of the specific (material) mass flux $Q = -K \text{Grad } p$ is compensated for by the time derivative of the volume ratio J . Furthermore, the momentum balance law (46b) defines the overall stress tensor of the biphasic system under study as $P_{\text{tot}} = -Jp g^{-1} F^{-T} + P$, where the pressure p is the Lagrange multiplier associated with the incompressibility and the saturation constraints.

The logical steps leading to (46a) and (46b) have been presented elsewhere (cf. e.g. [37, 19, 61, 33, 38, 39, 5, 40]), and will not be repeated here. In addition to them, the remodelling law (46c) supplies a further coupling among deformation, pressure, and plastic-like distortions.

Equations (46a)–(46c) shall be solved for simulating an *unconfined compression test* of the sample under study. This test represents a typical benchmark problem for investigating the elastic and hydraulic properties of biological tissues (cf. (46a) and (46b), respectively), and has been adapted here in order to also account for the reorganisation of the sample's internal structure (cf. (46c)). In the experiment simulated in this work, a specimen of tissue of cylindric shape is positioned between two rigid, parallel plates, and compressed. The two plates are impermeable to the fluid flow. The compression takes place in displacement control and, in particular, by displacing the upper plate according to a given loading ramp. The lower plate is instead kept fixed, and the specimen is clamped on it. The upper plate constitutes a frictionless glide surface for the specimen, whose upper boundary is thus allowed to deform radially in axial-symmetric way. The lateral boundary is assumed to be free of contact forces, thereby requiring that both the pressure and the radial component of the overall stress vanish on it (see (47b)).

By introducing a reference frame with origin O coinciding with the centre of the lower boundary of the sample, and orthonormal cartesian basis vectors $\{\Xi_I\}_{I=1}^3$ emanating

from O , such that Ξ_3 is the unit vector directed along the specimen's symmetry axis, the experiment described above is represented by the boundary conditions [5, 34]:

$$\begin{cases} \chi^3 = f \\ (-K \text{Grad } p) \cdot N = 0 \end{cases} \quad \text{on } \partial\mathcal{B}^{(u)}, \quad (47a)$$

$$\begin{cases} (-Jp\mathbf{g}^{-1}\mathbf{F}^{-T} + \mathbf{P}) \cdot N = 0 \\ p = 0 \end{cases} \quad \text{on } \partial\mathcal{B}^{(l)}, \quad (47b)$$

$$\begin{cases} \chi(X, t) - \chi(X, 0) = \mathbf{0} \\ (-K \text{Grad } p) \cdot N = 0 \end{cases} \quad \text{on } \partial\mathcal{B}^{(L)}. \quad (47c)$$

In (47a), χ^3 is the axial component of the motion, and f is the loading ramp

$$f(t) = \begin{cases} L - \frac{t}{T_{\text{ramp}}} u_T, & \text{for } t \in [0, T_{\text{ramp}}], \\ L - u_T, & \text{for } t \in]T_{\text{ramp}}, T_{\text{end}}], \end{cases} \quad (48)$$

where $u_T = 0.20$ mm is the target displacement imposed to the sample and $L = 1$ mm is the sample's initial length. The initial cross section of the sample has diameter $D = 3$ mm. The target displacement is reached at the end of the loading ramp, i.e., at $T_{\text{ramp}} = 20$ s, and is then kept constant until $T_{\text{end}} = 300$ s. Moreover, in (47a)–(47c), $\partial\mathcal{B}^{(u)}$, $\partial\mathcal{B}^{(l)}$ and $\partial\mathcal{B}^{(L)}$ are the upper, lateral and lower part of the boundary $\partial\mathcal{B}$, such that $\partial\mathcal{B} = \partial\mathcal{B}^{(u)} \sqcup \partial\mathcal{B}^{(l)} \sqcup \partial\mathcal{B}^{(L)}$. Finally, N is the unit vector normal to $\partial\mathcal{B}$.

It is assumed that, at the initial time, the sample finds itself in an undeformed state, with zero pressure, and in the absence of anelastic distortions. These requirements lead to the initial conditions

$$\chi(X, 0) = X, \quad \forall X \in \mathcal{B}, \quad (49a)$$

$$p(X, 0) = 0, \quad \forall X \in \mathcal{B}, \quad (49b)$$

$$\mathbf{V}(X, 0) = \mathbf{G}^{-1}(X) \quad \forall X \in \mathcal{B}. \quad (49c)$$

The numerical solution of (46a)–(46c), with (49a)–(49c) and (47a)–(47c), is achieved by performing Finite Element simulations. In particular, following [39, 5], (46a) and (46b) are put in weak form, and solved according to a given Finite Element scheme, while (46c) is solved only at the integration points of the finite elements. To this end, by searching for the motion χ and pressure p in the Sobolev spaces $(H^1(\mathcal{B} \times I, \mathcal{S}))^3$ and $H^1(\mathcal{B} \times I, \mathcal{S})$, respectively, and enforcing the boundary conditions (47a)–(47c), the model equations (46a)–(46c) are reformulated as

$$\begin{aligned} \mathcal{F}_\chi &= \hat{\mathcal{F}}_\chi(\chi, p, V) \\ &= \int_{\mathcal{B}} \hat{\mathbf{P}}(\chi, p, V) : \mathbf{g} \text{Grad } \tilde{\mathbf{u}} = 0, \end{aligned} \quad (50a)$$

$$\begin{aligned} \mathcal{F}_p &= \hat{\mathcal{F}}_p(\chi, p, V) \\ &= \int_{\mathcal{B}} \{ (\text{Grad } \tilde{p}) \hat{\mathbf{K}}(\chi, V) (\text{Grad } p) + \tilde{p} j \} = 0, \end{aligned} \quad (50b)$$

$$\mathcal{F}_V = \hat{\mathcal{F}}_V(\chi, V) = \text{sym}(\dot{\mathbf{V}} V^{-1}) + \hat{\mathbf{R}}(\chi, V) = \mathbf{0}, \quad (50c)$$

where $\tilde{\mathbf{u}}$ and \tilde{p} are the test functions associated with the velocity and pressure and are sometimes referred to as “virtual velocity” and “virtual pressure”, respectively. We notice that the functionals $\hat{\mathcal{F}}_\chi$ and $\hat{\mathcal{F}}_p$ depend linearly on the virtual fields $\tilde{\mathbf{u}}$ and \tilde{p} . However, for the sake of a lighter notation, we have omitted this dependence in their definitions.

5 Results

In this section, we present and discuss the main results of our simulations (see Figures 2–6). In particular, we show (i) how remodelling modulates the mechanical and hydraulic response of the tissue, and (ii) how the fibre reinforcement, which makes the tissue transversely isotropic, influences the evolution of the anelastic distortions. To highlight the consequences of remodelling, we run a set of simulations in which remodelling is switched off, and we compare the corresponding results with those stemming from the set of simulations in which the models M1 and M2 are implemented. Moreover, in order to see the role played by the fibre reinforcement, we compare the results predicted by the model M1, in which an ideal isotropic tissue without fibres is simulated, with those predicted by the model M2, in which the presence of the fibres is accounted for. In all the plots (Figures 2–6), we evaluate the physical quantity of interest at the point X_U of Cartesian coordinates given by (1.3, 0.0, 1.0) [mm], which is on the upper boundary and close to the lateral boundary of the sample.

In Figure 2a, we report the time trend of the magnitude of the (spatial) filtration velocity, $\|\mathbf{q}(X_U, t)\|$, evaluated at the point X_U for $t \in [0, T_{\text{end}}]$, where we let T_{end} be arbitrarily greater than T_{ramp} . We show both the case of no remodelling and the case of remodelling, as described by the models M1 and M2. In the absence of remodelling, the magnitude of the filtration velocity grows monotonically until the target displacement is reached, i.e., until $t = T_{\text{ramp}}$. Then, it relaxes asymptotically towards zero for increasing time. When remodelling occurs, the trend of $\|\mathbf{q}(X_U, t)\|$ depends on whether or not the fibres are accounted for. In the simulation performed by applying the model M1, the influence of remodelling on $\|\mathbf{q}(X_U, t)\|_{\text{M1}}$ is twofold: on the one hand, it lowers considerably the maximum value of $\|\mathbf{q}(X_U, t)\|$, which is however attained at $t = T_{\text{ramp}}$, and, on the other hand, it leads to a much slower relaxation time. Hence, even though $\|\mathbf{q}(X_U, t)\|_{\text{M1}}$ decreases monotonically towards zero, the curve associated with M1 intersects the curve of no remodelling, and it holds that

$$\|\mathbf{q}(X_U, t)\|_{\text{M1}} \geq \|\mathbf{q}(X_U, t)\|_{\text{no-rem}}, \quad (51)$$

for all $t \geq T_1$, with $T_1 > T_{\text{ramp}}$ being the time at which the two curves intersect each other. The simulation performed considering the model M2 leads, instead, to quite different

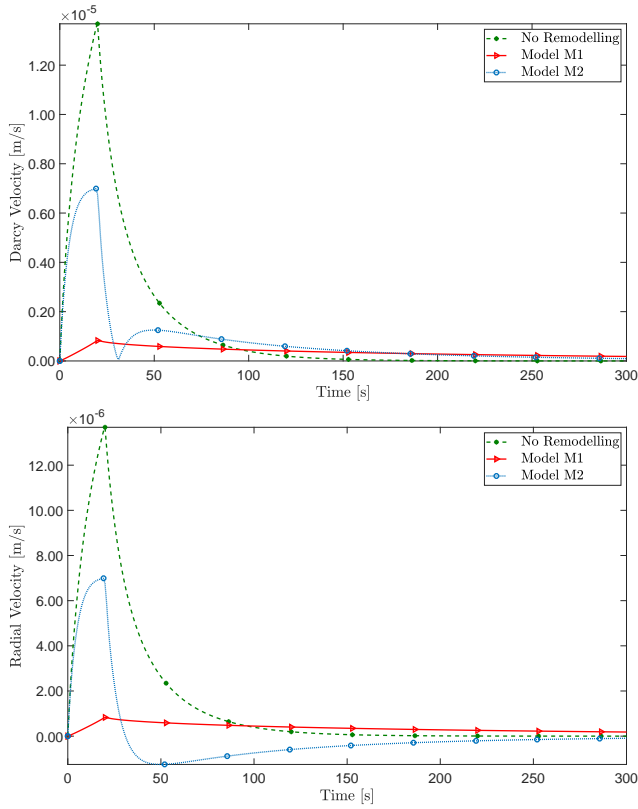


Fig. 2 Norm of Darcy velocity vs time (a) and radial component of Darcy velocity vs time (b), evaluated at the point X_U of Cartesian coordinates (1.3, 0.0, 1.0) [mm]. The anisotropic model predicts an inversion of the filtration velocity, which yields thus an inflow of fluid after a critical instant of time is reached. This behaviour is not captured by the isotropic model M1.

results. First of all, the maximum value of $\|q(X_U, t)\|_{M2}$, always attained at $T = T_{\text{ramp}}$, is smaller than the one reached in the case of no remodelling and bigger than the one predicted by M1. Moreover, the relaxation of $\|q(X_U, t)\|_{M2}$ towards zero is slower than that observed in the case of no remodelling, but slightly faster than the one obtained by employing the model M1. The most noticeable results, however, are given by the loss of monotonicity of $\|q(X_U, t)\|_{M2}$ in the interval $[T_{\text{ramp}}, T_{\text{end}}[$, and by the presence of the point of non-differentiability, hereafter denoted by T_c , between T_{ramp} and $t = 50$ s. This behaviour is due to the fact that, when remodelling occurs and the anisotropy of the fibre pattern is considered, the radial component of the filtration velocity decreases for $t > T_{\text{ramp}}$, becomes negative until it attains a global minimum and, subsequently, it grows asymptotically towards zero for a sufficiently long time (see Figure 2b).

The change of sign in the radial velocity may be interpreted as a “syringe effect”, thereby meaning that, for $t > T_c$, the fluid tends to flow back into the tissue. Since the fluid filtration velocity complies with Darcy’s law, this behaviour is accompanied by a change of sign of the radial pressure gradient, which implies that the pressure at X_U becomes

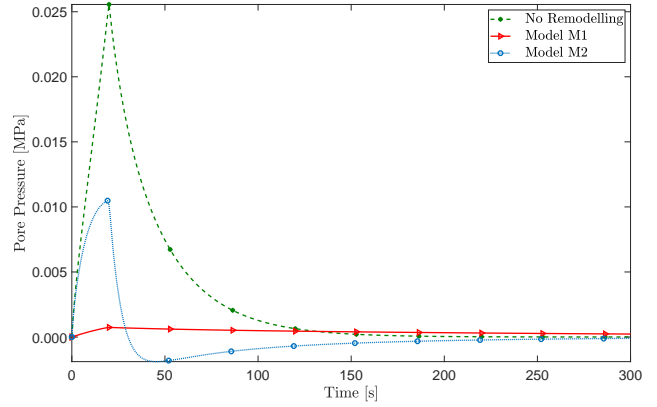


Fig. 3 Pressure vs time, $p(X_U, t)$, evaluated at the point X_U of Cartesian coordinates (1.3, 0.0, 1.0) [mm]. The isotropic model M1 predicts a dramatic decrease of pressure due to the progression of remodelling. In the case of the model M2, instead, the interplay between the evolution of the plastic distortions and the tissue’s anisotropy contains the pressure fall and induces a loss of monotonicity in the time trend. This is consistent with the inversion of the filtration velocity observed in Figure 2.

smaller than zero for $t > T_c$ (we recall, indeed, that our boundary conditions prescribe that, on the lateral boundary of the sample, the pressure is zero at all times). This observation seems to be supported by the results shown in Figure 3. In the absence of remodelling, pressure grows until a global maximum is reached, and it relaxes then towards zero for increasing time. A qualitatively similar trend is also observed when remodelling is switched on and the model M1 is used, even though the maximum value of pressure is much smaller than the one obtained in the case of no remodelling. The model M1 predicts, indeed, that $[p(X_U, t)]_{M1}$ consists of two monotonic branches, one increasing over the interval $[0, T_{\text{ramp}}]$ and the other one decreasing over $[T_{\text{ramp}}, T_{\text{end}}[$. The decreasing branch intersects the relaxing branch of the pressure curve of no remodelling and tends towards zero more slowly than the latter one. The curve determined by simulating the model M2 grows rather steeply until the maximum pressure is attained, and this maximum places itself in between the values obtained in the case of no remodelling and that of the model M1, respectively. Then, $[p(X_U, t)]_{M2}$ decreases much faster than it happens in the other cases, becomes negative, and reaches a global minimum. Afterwards it grows again, and it then tends to zero from below at a rate comparable with that of no remodelling. We remark that the instant of time at which pressure equals zero coincides with T_c , i.e., the time at which the radial component of the filtration velocity changes its sign.

In Figure 4, we study the time trend of porosity at X_U . We notice that, both in the case of no remodelling and in the case of the model M1, porosity decreases monotonically in time. In the absence of remodelling, porosity varies very smoothly, and the amplitude of the variation between its ini-

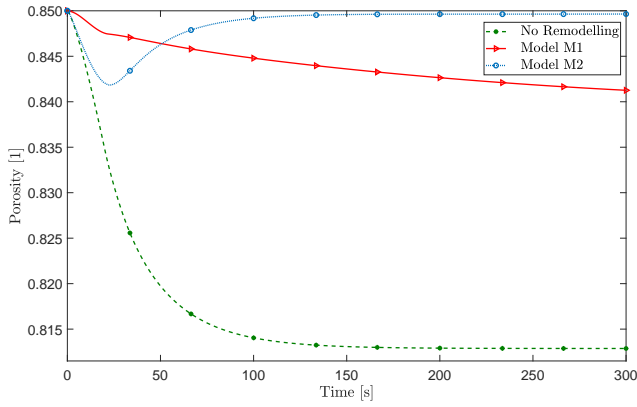


Fig. 4 Porosity vs time, $1 - \Phi_{sv}(X_U)/J(X_U, t)$, evaluated at the point X_U of Cartesian coordinates (1.3, 0.0, 1.0) [mm]. Whereas the case of no remodelling and the model M1 predict quantitatively different, but qualitatively similar, results, the model M2 is characterised by a trend that is both quantitatively and qualitatively different from the other two. The loss of monotonicity is, in fact, consistent with that of Figures 2 and 3, and represents an opening of the tissue's pores (with corresponding increase of porosity) on the way towards the stationary state.

tial and asymptotic values is bigger than in the other case. The model M1, in turn, predicts a rather pronounced change of slope of the porosity curve, and the asymptotic value of porosity is reached more slowly. A quite different behaviour can be observed when the tissue's anisotropy is accounted for. Indeed, in accordance with the inversion of the fluid filtration velocity (see Figure 2) and the change of sign of the pressure (see Figure 3), the model M2 prescribes that porosity varies in time in a non-monotonic way. More specifically, it decreases until it comes to a global minimum, which corresponds to the end of the loading ramp, and then it grows towards a stationary value. This behaviour is consistent with the fact that, to permit the inflow of fluid, the tissue must increase its porosity, and it seems to be a consequence of the interplay between the tissue's anisotropy and the evolution of the anelastic distortions.

In terms of F_p , a measure of the magnitude of plastic-like distortions is the Frobenius norm of the anelastic strain tensor

$$E_p = \frac{1}{2} [F_p^T \cdot F_p - G]. \quad (52)$$

Since it holds that F_p is the inverse of Π , E_p may be rewritten as

$$E_p = \frac{1}{2} [\Pi^{-T} \cdot \Pi^{-1} - G] = -\mathcal{A}_\Pi, \quad (53)$$

where \mathcal{A}_Π is the Almansi-Euler-like strain tensor associated with Π . Finally, by enforcing the polar decomposition $\Pi = V \cdot R$, E_p becomes

$$E_p = \frac{1}{2} [V^{-1} \cdot V^{-1} - G]. \quad (54)$$

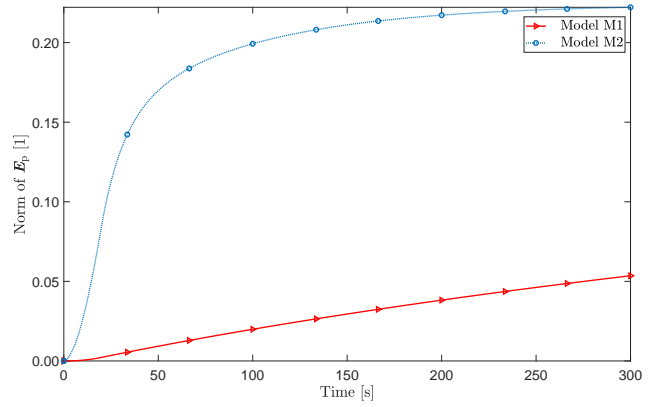


Fig. 5 Frobenius norm of $E_p = \frac{1}{2} [V^{-1} \cdot V^{-1} - G]$ vs time, $\|E_p(X_U, t)\|$, evaluated at the point X_U of Cartesian coordinates (1.3, 0.0, 1.0) [mm]. The magnitude of the plastic strains is bigger in the transversely isotropic model M2. In the isotropic model M1, instead, the plastic strains are rather small, but they tend to the stationary state much more slowly than predicted by the model M2.

Equation (53) suggests which tensor field should be used to address remodelling within the theory of uniformity [15, 50, 7, 54].

The Frobenius norm of E_p is now evaluated at X_U and its variation in time is reported in Figure 5. We notice that the magnitude of the anelastic distortions as predicted by the model M2 is much bigger than that obtained by the model M1. Thus, the anisotropy of the tissue seems to enhance the growth of the plastic distortions, whose magnitude increases quite rapidly and tends to approach a stationary value. In the case of the model M1, instead, $\|E_p(X_U, t)\|$ grows much more slowly (and almost linearly) towards a stationary value.

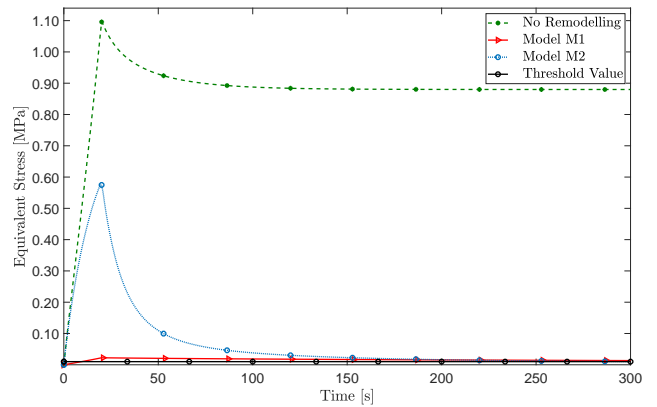


Fig. 6 Equivalent stress vs time, evaluated at the point X_U of Cartesian coordinates (1.3, 0.0, 1.0) [mm]. The equivalent stress is the Frobenius norm of the deviatoric part of the constitutive Cauchy stress tensor, i.e., $\|\text{dev} \sigma\|$, with $\sigma = J^{-1} F S F^T$. The 2nd Piola-Kirchhoff stress tensor S is given by (38) for the model M1, and by (41) both for the model M2 and for the case of no remodelling (in which, however, the identity $V = G^{-1}$ applies).

Finally, we investigate how the onset of plastic distortions modulates the stress borne by the tissue. To this end, we plot in Figure 6 the von Mises equivalent stress at X_U , and we notice that the curve corresponding to the model M1 is, until about 200 s, bounded from above by the curve pertaining to the model M2. This means that, even though the plastic distortions are characterised by a magnitude of E_p that is bigger in the anisotropic case than in the isotropic one, the level of stress reached in the first case is higher. We remark that the onset of remodelling occurs only when the von Mises equivalent stress, $\|\text{dev}\sigma\|$, overcomes the yield stress, σ_Y . In fact, there exists an instant of time such that the condition of incipient remodelling, i.e., $\|\text{dev}\sigma\| = \sigma_Y$, is verified, and the von Mises equivalent stress is bigger than σ_Y for all subsequent times. To highlight this behaviour, we plotted in Figure 6 the yield stress (which is constant in time in this work), and we showed that, in all the considered cases, the von Mises equivalent stress exceeds the yield stress after a quite short interval of time.

6 Conclusions

In this work, we employed an inhomogeneous and transversely isotropic poroplastic model of fibre-reinforced biological tissue in order to study how the variation of the tissue's internal structure (i.e., the process of remodelling), which manifests itself through the onset and evolution of anelastic distortions, is influenced by the material symmetries of the tissue itself.

For our purposes, we rephrased the poroelastic model of hydrated, fibre-reinforced tissues summarised in [19, 61] in order to account for the presence of anelastic distortions (the definition of the hyperelastic strain energy energy is developed from [24, 19] and the tissue's permeability has been adapted from [23, 22, 19, 61]). Then, we formulated and solved numerically the two different descriptions of structural remodelling denoted by model M1 and model M2. We recall that, while the tissue has been simulated as inhomogeneous and transversely isotropic both in the case of the model M2 and in the reference case of no remodelling, it has been regarded as inhomogeneous but isotropic in the model M1. We emphasise that this idealisation serves as a basis for comparison with the transversely isotropic model M2, and has been done to highlight the interplay between the tissue's material symmetries and the development of plastic distortions. These, indeed, drive an evolution of the group of material symmetries, but they do not change it (see [12, 13] for further details).

Among the obtained results, represented graphically in Figures 2–6, we give prominence to the “syringe effect” discussed in Section 5, which is observed in our simulations only when remodelling occurs in the tissue modelled as an inhomogeneous and transversely isotropic material (cf. model

M2). Such effect seems to be an evidence of the change of the tissue's mechanical and hydraulic behaviour. Such alteration of material response could characterise a diseased or damaged tissue, and could thus also provide some indications on how the tissue might behave in non-physiological conditions.

Finally, since the observed changes of material behaviour occurs both qualitatively and quantitatively in the case of anisotropy (while the change is only quantitative in the case of isotropy), our results could be used for studying the interplay between growth and remodelling in anisotropic tissues. For example, this could be of interest for elaborating more detailed and more accurate models of tumour growth, in which the onset of remodelling has appreciable consequences on the tumour evolution [49, 48].

Appendix A: Fourth-order tensors

The notation adopted in the following is taken from [17]. Let $[T\mathcal{B}]_1^1$, $[T\mathcal{B}]_1^1$, $[T\mathcal{B}]_0^2$, and $[T\mathcal{B}]_2^2$ denote the spaces of all second-order tensors which, as bilinear maps, read

$$\mathbf{A} : T^*\mathcal{B} \times T\mathcal{B} \rightarrow \mathbb{R}, \quad (55a)$$

$$\mathbf{B} : T\mathcal{B} \times T^*\mathcal{B} \rightarrow \mathbb{R}, \quad (55b)$$

$$\mathbf{T} : T^*\mathcal{B} \times T^*\mathcal{B} \rightarrow \mathbb{R}, \quad (55c)$$

$$\mathbf{Q} : T\mathcal{B} \times T\mathcal{B} \rightarrow \mathbb{R}, \quad (55d)$$

respectively. Let also $([T\mathcal{B}]_0^2, \text{sym})$ and $([T\mathcal{B}]_2^2, \text{sym})$ be, respectively, the subspaces of $[T\mathcal{B}]_0^2$ and $[T\mathcal{B}]_2^2$ of all symmetric, second-order tensors. The elements of $[T\mathcal{B}]_1^1$ and $[T\mathcal{B}]_1^1$ can be written as linear maps from $T\mathcal{B}$ into itself, and from $T^*\mathcal{B}$ into itself, respectively, while the elements of $[T\mathcal{B}]_0^2$, and $[T\mathcal{B}]_2^2$ can be written as linear maps from $T^*\mathcal{B}$ into $T\mathcal{B}$, and from $T\mathcal{B}$ into $T^*\mathcal{B}$, respectively.

Let us also consider the spaces $[T\mathcal{B}]_2^2$ and $[T\mathcal{B}]_2^2$ of all fourth-order tensors of the type

$$\mathbb{T} \in [T\mathcal{B}]_2^2, \quad \mathbb{T} : T^*\mathcal{B} \times T^*\mathcal{B} \times T\mathcal{B} \times T\mathcal{B} \rightarrow \mathbb{R},$$

$$\mathbb{Q} \in [T\mathcal{B}]_2^2, \quad \mathbb{Q} : T\mathcal{B} \times T\mathcal{B} \times T^*\mathcal{B} \times T^*\mathcal{B} \rightarrow \mathbb{R}.$$

An element of $[T\mathcal{B}]_2^2$ can also be represented as a linear map from $[T\mathcal{B}]_0^2$ into $[T\mathcal{B}]_0^2$. Analogously, an element of $[T\mathcal{B}]_2^2$ can be represented as a linear map from $[T\mathcal{B}]_2^2$ into $[T\mathcal{B}]_2^2$. For instance, the fourth-order tensor

$$\begin{aligned} \mathbb{I} : [T\mathcal{B}]_0^2 &\rightarrow ([T\mathcal{B}]_0^2, \text{sym}), \\ \mathbb{I} &= \frac{1}{2} (\mathbf{I} \otimes \mathbf{I} + \mathbf{I} \otimes \mathbf{I}), \end{aligned} \quad (57)$$

where $\mathbf{I} : T\mathcal{B} \rightarrow T\mathcal{B}$ is the identity tensor in $T\mathcal{B}$, returns the symmetric part of the element of $[T\mathcal{B}]_0^2$ to which it is applied. Given two tensors $\mathbf{A}, \mathbf{D} \in [T\mathcal{B}]_1^1$, the representation of the tensor products $\mathbf{A} \otimes \mathbf{D}$ and $\mathbf{A} \otimes \mathbf{D}$ in index notation reads $[\mathbf{A} \otimes \mathbf{D}]_{MN}^{AB} = A_M^A D_N^B$ and $[\mathbf{A} \otimes \mathbf{D}]_{MN}^{AB} = A_N^A D_M^B$

[9]. Accordingly, in index notation, \mathbb{I} is represented by the expression

$$\mathbb{I}^{AB}_{MN} = \frac{1}{2} \left(\delta^A_M \delta^B_N + \delta^A_N \delta^B_M \right). \quad (58)$$

Thus, for every $\mathbf{T} \in [T\mathcal{B}]_0^2$, it holds that

$$\mathbb{I} : \mathbf{T} = \frac{1}{2} \left(\mathbf{T} + \mathbf{T}^T \right) = \text{sym}(\mathbf{T}), \quad (59)$$

where the symbol “ \cdot ” stands for “double contraction”. In index notation, it reads $(\mathbb{I} : \mathbf{T})^{AB} = \mathbb{I}^{AB}_{MN} T^{MN} = [\text{sym}(\mathbf{T})]^{AB}$. By definition, \mathbb{I} is the identity fourth-order tensor over the space $([T\mathcal{B}]_0^2, \text{sym})$. From here on, we consider only the restrictions of the fourth-order tensors of $[T\mathcal{B}]_0^2$ onto $([T\mathcal{B}]_0^2, \text{sym})$. For every $\mathbf{T} \in ([T\mathcal{B}]_0^2, \text{sym})$, the fourth-order tensor

$$\begin{aligned} \mathbb{K}^* : ([T\mathcal{B}]_0^2, \text{sym}) &\rightarrow ([T\mathcal{B}]_0^2, \text{sym}), \\ \mathbb{K}^* &= \frac{1}{3} \mathbf{C}^{-1} \otimes \mathbf{C} \end{aligned} \quad (60)$$

extracts the spherical part of \mathbf{T} with respect to the metric \mathbf{C} , i.e.,

$$\mathbb{K}^* : \mathbf{T} = \frac{1}{3} \text{tr}(\mathbf{C}\mathbf{T}) \mathbf{C}^{-1}. \quad (61)$$

The deviatoric part of \mathbf{T} with respect to the metric \mathbf{C} is obtained by subtracting $\mathbb{K}^* : \mathbf{T}$ to \mathbf{T} . This operation can be represented by the application of the fourth-order tensor

$$\begin{aligned} \mathbb{M}^* : ([T\mathcal{B}]_0^2, \text{sym}) &\rightarrow ([T\mathcal{B}]_0^2, \text{sym}) \\ \mathbb{M}^* &= \mathbb{I} - \mathbb{K}^*, \end{aligned} \quad (62)$$

to \mathbf{T} i.e.,

$$\mathbb{M}^* : \mathbf{T} = (\mathbb{I} - \mathbb{K}^*) : \mathbf{T} = \mathbf{T} - \frac{1}{3} \text{tr}(\mathbf{C}\mathbf{T}) \mathbf{C}^{-1}. \quad (63)$$

Clearly, it holds that $\text{tr}[\mathbf{C}(\mathbb{M}^* : \mathbf{T})] = 0$. We remark that, by their own definition, \mathbb{K}^* and \mathbb{M}^* constitute the partition of unity, i.e., $\mathbb{I} = \mathbb{K}^* + \mathbb{M}^*$.

In analogous manner, we introduce the identity fourth-order tensor over the space $([T\mathcal{B}]_2^0, \text{sym})$, i.e.,

$$\begin{aligned} \mathbb{I}^T : ([T\mathcal{B}]_2^0, \text{sym}) &\rightarrow ([T\mathcal{B}]_2^0, \text{sym}), \\ \mathbb{I}^T &= \frac{1}{2} \left(\mathbf{I}^T \otimes \mathbf{I}^T + \mathbf{I}^T \otimes \mathbf{I}^T \right), \end{aligned} \quad (64)$$

where $\mathbf{I}^T : T^*\mathcal{B} \rightarrow T^*\mathcal{B}$ is the identity tensor in $T^*\mathcal{B}$. For every $\mathbf{Q} \in ([T\mathcal{B}]_2^0, \text{sym})$ it holds that

$$\mathbb{I}^T : \mathbf{Q} = \frac{1}{2} \left(\mathbf{Q} + \mathbf{Q}^T \right) \equiv \mathbf{Q}. \quad (65)$$

The spherical and the deviatoric parts of \mathbf{Q} with respect to the inverse metric \mathbf{C}^{-1} are extracted by employing the fourth-order tensors

$$\begin{aligned} \mathbb{K}^{*T} : ([T\mathcal{B}]_2^0, \text{sym}) &\rightarrow ([T\mathcal{B}]_2^0, \text{sym}), \\ \mathbb{K}^{*T} &= \frac{1}{3} \mathbf{C} \otimes \mathbf{C}^{-1}, \end{aligned} \quad (66)$$

and

$$\begin{aligned} \mathbb{M}^{*T} : ([T\mathcal{B}]_2^0, \text{sym}) &\rightarrow ([T\mathcal{B}]_2^0, \text{sym}), \\ \mathbb{M}^{*T} &= \mathbb{I}^T - \mathbb{K}^{*T}, \end{aligned} \quad (67)$$

respectively, which are such that

$$\mathbb{K}^{*T} : \mathbf{Q} = \frac{1}{3} \text{tr}(\mathbf{C}^{-1} \mathbf{Q}) \mathbf{C}, \quad (68)$$

$$\mathbb{M}^{*T} : \mathbf{Q} = (\mathbb{I}^T - \mathbb{K}^{*T}) : \mathbf{Q} = \mathbf{Q} - \frac{1}{3} \text{tr}(\mathbf{C}^{-1} \mathbf{Q}) \mathbf{C}. \quad (69)$$

In this case, it holds that $\text{tr}[\mathbf{C}^{-1}(\mathbb{M}^{*T} : \mathbf{Q})] = 0$.

Finally, we introduce the fourth-order tensor

$$\begin{aligned} \mathbb{I}^{\sharp*} : ([T\mathcal{B}]_2^0, \text{sym}) &\rightarrow ([T\mathcal{B}]_2^0, \text{sym}), \\ \mathbb{I}^{\sharp*} &= \frac{1}{2} \left(\mathbf{C}^{-1} \otimes \mathbf{C}^{-1} + \mathbf{C}^{-1} \otimes \mathbf{C}^{-1} \right). \end{aligned} \quad (70)$$

For every $\mathbf{Q} \in ([T\mathcal{B}]_2^0, \text{sym})$, it holds that

$$\mathbb{I}^{\sharp*} : \mathbf{Q} = \mathbf{C}^{-1} \mathbf{Q} \mathbf{C}^{-1}. \quad (71)$$

In index notation, Equation (71) implies $(\mathbb{I}^{\sharp*} : \mathbf{Q})^{AB} = (\mathbf{C}^{-1})^{AM} \mathbf{Q}_{MN} (\mathbf{C}^{-1})^{NB}$, which means that $\mathbb{I}^{\sharp*}$ raises the indices of \mathbf{Q} through the inverse metric tensor \mathbf{C}^{-1} rather than through \mathbf{G}^{-1} , the latter being the inverse of the metric tensor \mathbf{G} in the undeformed configuration. In analogy with \mathbb{K}^* and \mathbb{M}^* , we also consider the fourth-order tensors

$$\begin{aligned} \mathbb{K}^{\sharp*} : ([T\mathcal{B}]_2^0, \text{sym}) &\rightarrow ([T\mathcal{B}]_2^0, \text{sym}), \\ \mathbb{K}^{\sharp*} &= \frac{1}{3} \mathbf{C}^{-1} \otimes \mathbf{C}^{-1}, \end{aligned} \quad (72a)$$

$$\begin{aligned} \mathbb{M}^{\sharp*} : ([T\mathcal{B}]_2^0, \text{sym}) &\rightarrow ([T\mathcal{B}]_2^0, \text{sym}), \\ \mathbb{M}^{\sharp*} &= \mathbb{I}^{\sharp*} - \mathbb{K}^{\sharp*}. \end{aligned} \quad (72b)$$

For every $\mathbf{Q} \in ([T\mathcal{B}]_2^0, \text{sym})$, we obtain

$$\mathbb{K}^{\sharp*} : \mathbf{Q} = \frac{1}{3} \text{tr}(\mathbf{C}^{-1} \mathbf{Q}) \mathbf{C}^{-1}, \quad (73a)$$

$$\mathbb{M}^{\sharp*} : \mathbf{Q} = \mathbf{C}^{-1} \mathbf{Q} \mathbf{C}^{-1} - \frac{1}{3} \text{tr}(\mathbf{C}^{-1} \mathbf{Q}) \mathbf{C}^{-1}. \quad (73b)$$

Note that the second-order tensor $\mathbb{M}^{\sharp*} : \mathbf{Q}$ is deviatoric in the sense that $\text{tr}[\mathbf{C}(\mathbb{M}^{\sharp*} : \mathbf{Q})] = 0$.

Compliance with ethical standards

Conflict of interest: The authors declare that they have no conflict of interest.

References

1. Ambrosi, D., Guana, F.: Stress-modulated growth. *Math. Mech. Solids* **12**, 319–342 (2007)
2. Ambrosi, D., Guillou, A., Martino, E.S.D.: Stress-modulated remodelling of a non-homogeneous body. *Biomechanics and Modeling in Mechanobiology* **1**, 63–76 (2007)
3. Ateshian, G.A.: On the theory of reactive mixtures for modeling biological growth. *Biomech Model Mechanobiol.* **6**(6), 423–445 (2007)
4. Bachrach, N.M., Mow, V.C., Guilak, F.: Incompressibility of the solid matrix of articular cartilage under high hydrostatic pressures. *Journal of Biomechanics* **31**, 445–451 (1998)
5. Carfagna, M., Grillo, A.: The spherical design algorithm in the numerical simulation of biological tissues with statistical fibre-reinforcement. *Computing and Visualization in Science* pp. 1–28 (2017). DOI 10.1007/s00791-017-0278-6. URL <http://dx.doi.org/10.1007/s00791-017-0278-6>
6. Ciarletta, P., Ambrosi, D., Maugin, G.A., Preziosi, L.: Mechano-transduction in tumour growth modelling. *Eur. Phys. J. E* **36**, 23–31 (2013)
7. Cleja-Tigoiu, S., Maugin, G.A.: Eshelby's stress tensors in finite elastoplasticity. *Acta Mechanica* **139**, 231–249 (2000)
8. Crevacore, E., Di Stefano, S., Grillo, A.: Coupling among deformation, fluid flow, structural reorganisation and fibre reorientation in fibre-reinforced, transversely isotropic biological tissues. *International Journal of Non-Linear Mechanics* **111**, 1–13 (2019). DOI 10.1016/j.ijnonlinmec.2018.08.022
9. Curnier, A., He, Q.C., Zysset, P.: Conewise linear elastic materials. *Journal of Elasticity* **37**, 1–38 (1995)
10. Di Stefano, S., Ramírez-Torres, A., Penta, R., Grillo, A.: Self-influenced growth through evolving material inhomogeneities. *International Journal of Non-Linear Mechanics* **106**, 174–187 (2018). DOI 10.1016/j.ijnonlinmec.2018.08.003
11. DiCarlo, A., Quiligotti, S.: Growth and balance. *Mechanics Research Communications* **29**, 449–456 (2002)
12. Epstein, M.: The split between remodelling and aging. *International Journal of Non-Linear Mechanics* **44**(6), 604–609 (2009). DOI 10.1016/j.ijnonlinmec.2009.02.005
13. Epstein, M.: Mathematical characterization and identification of remodeling, growth, aging and morphogenesis. *Journal of the Mechanics and Physics of Solids* **84**, 72–84 (2015). DOI 10.1016/j.jmps.2015.07.009
14. Epstein, M., Elzanowski, M.: *Material Inhomogeneities and their Evolution – A Geometric Approach*. Springer, Berlin, Heidelberg, New York (2004)
15. Epstein, M., Maugin, G.A.: On the geometrical material structure of anelasticity. *Acta Mechanica* **115**(1-4), 119–131 (1996). DOI 10.1007/bf01187433
16. Epstein, M., Maugin, G.A.: Thermomechanics of volumetric growth in uniform bodies. *International Journal of Plasticity* **16**(7-8), 951–978 (2000). DOI 10.1016/s0749-6419(99)00081-9
17. Federico, S.: Covariant formulation of the tensor algebra of non-linear elasticity. *International Journal of Nonlinear Mechanics* **47**, 273–284 (2012)
18. Federico, S., Gasser, T.C.: Non-linear elasticity of biological tissues with statistical fibre orientation. *Journal of the Royal Society Interface* **7**, 955–966 (2010)
19. Federico, S., Grillo, A.: Elasticity and permeability of porous fibre-reinforced materials under large deformations. *Mechanics of Materials* **44**, 58–71 (2012)
20. Federico, S., Grillo, A.: *Linear Elastic Composites with Statistically Oriented Spheroidal Inclusions*, pp. 307–346. Springer, Berlin (2018)
21. Federico, S., Grillo, A., La Rosa, G., Giaquinta, G., Herzog, W.: A transversely isotropic, transversely homogeneous microstructural-statistical model of articular cartilage. *Journal of Biomechanics* **38**, 2008–2018 (2005)
22. Federico, S., Herzog, W.: On the anisotropy and inhomogeneity of permeability in articular cartilage. *Biomechanics and Modeling in Mechanobiology* **7**, 367–378 (2008)
23. Federico, S., Herzog, W.: On the permeability of fibre-reinforced porous materials. *International Journal of Solids and Structures* **45**, 2160–2172 (2008)
24. Federico, S., Herzog, W.: Towards an analytical model of soft tissues. *Journal of Biomechanics* **41**, 3309–3313 (2008)
25. Fung, Y.C.: *Biomechanics. Motion, Flow, Stress, and Growth*. Springer-Verlag, New York, USA (1990)
26. Ganghoffer, J.: On eshelby tensors in the context of the thermodynamics of open systems: application to volumetric growth. *International Journal of Engineering Science* **48**(12), 2081–2098 (2010)
27. Garcia, D., Zysset, P.K., Charlebois, M., Curnier, A.: A three-dimensional elastic plastic damage constitutive law for bone tissue. *Biomech Model Mechanobiol* **8**, 149–165 (2009)
28. Garikipati, K., Arruda, E.M., Grosh, K., Narayanan, H., Calve, S.: A continuum treatment of growth in biological tissue: the coupling of mass transport and mechanics. *Journal of the Mechanics and Physics of Solids* **52**, 1595–1625 (2004)
29. Garikipati, K., Olbering, J.E., Narayanan, H., Arruda, E.M., Grosh, K., Calve, S.: Biological remodelling: Stationary energy, configurational change, internal variables and dissipation. *Journal of the Mechanics and Physics of Solids* **54**, 1493–1515 (2006)
30. Gasser, T.C., Ogden, R.W., Holzapfel, G.A.: Hyperelastic modelling of arterial layers with distributed collagen fibre orientations. *Journal of the Royal Society Interface* **3**, 15–35 (2006)
31. Giverso, C., Preziosi, L.: Modelling the compression and reorganization of cell aggregates. *Math. Med. Biol.* **29**, 181–204 (2012)
32. Goriely, A.: *The Mathematics and Mechanics of Biological Growth*. Springer, Heidelberg, Germany (2017)
33. Grillo, A., Carfagna, M., Federico, S.: The Darcy-Forchheimer law for modelling fluid flow in biological tissues. *Theoret. Appl. Mech. TEOPM7* **41**(4), 283–322 (2014)
34. Grillo, A., Carfagna, M., Federico, S.: Non-Darcian flow in fibre-reinforced biological tissues. *Meccanica* **52**, 3299–3320 (2017)
35. Grillo, A., Carfagna, M., Federico, S.: An Allen–Cahn approach to the remodelling of fibre-reinforced anisotropic materials. *Journal of Engineering Mathematics* **109**(1), 139–172 (2018). DOI 10.1007/s10665-017-9940-8. URL <https://doi.org/10.1007/s10665-017-9940-8>
36. Grillo, A., Federico, S., Wittum, G.: Growth, mass transfer, and remodeling in fiber-reinforced, multi-constituent materials. *International Journal of Non-Linear Mechanics* **47**, 388–401 (2012)
37. Grillo, A., Giverso, C., Favino, M., Krause, R., Lampe, M., Wittum, G.: Mass transport in porous media with variable mass. In: J.M.P.Q.D. et al. (ed.) *Numerical Analysis of Heat and Mass Transfer in Porous Media*, pp. 27–61. Springer-Verlag, Berlin, Heidelberg, Germany (2012). DOI 10.1007/978-3-642-30532-0-2
38. Grillo, A., Gualy, A., Giverso, C., Federico, S.: Non-linear model for compression tests on articular cartilage. *Journal of Biomechanical Engineering* **137**, 071,004–1–071,004–8 (2015)
39. Grillo, A., Prohl, R., Wittum, G.: A poroplastic model of structural reorganisation in porous media of biomechanical interest. *Continuum Mechanics and Thermodynamics* **28**, 579–601 (2016)
40. Grillo, A., Prohl, R., Wittum, G.: A generalised algorithm for anelastic processes in elastoplasticity and biomechanics. *Mathematics and Mechanics of Solids* **22**(3), 502–527 (2017). DOI 10.1177/1081286515598661
41. Holmes, M.H., Mow, V.C.: The nonlinear characteristics of soft gels and hydrated connective tissues in ultrafiltration. *Journal of Biomechanics* **23**, 1145–1156 (1990)
42. Lanir, Y.: Constitutive equations for fibrous connective tissues. *Journal of Biomechanics* **16**, 1–12 (1983)
43. Loret, B., Simões, F.M.F.: A framework for deformation, generalized diffusion, mass transfer and growth in multi-species multiphase biological tissues. *European Journal of Mechanics A/Solids* **24**, 757–781 (2005)

44. Lu, Y., Lekszycki, T.: Modelling of bone fracture healing: influence of gap size and angiogenesis into bioresorbable bone substitute. *Mathematics and Mechanics of Solids* **0**(0), 1081286516653,272 (0). DOI 10.1177/1081286516653272. URL <http://dx.doi.org/10.1177/1081286516653272>
45. Lubarda, V.A., Hoger, A.: On the mechanics of solids with a growing mass. *International Journal of Solids and Structures* **39**, 4627–4664 (2002)
46. Lubliner, J.: *Plasticity Theory*. Dover Publications, Inc., Mineola, NY (2008)
47. Marsden, J.E., Hughes, T.J.R.: *Mathematical Foundations of Elasticity*. Dover Publications, Inc., New York (1983)
48. Mascheroni, P., Carfagna, M., Grillo, A., Boso, D., Schrefler, B.: An avascular tumor growth model based on porous media mechanics and evolving natural states. *Mathematics and Mechanics of Solids* **23**(4), 686–712 (2017). DOI 10.1177/1081286517711217
49. Mascheroni, P., Stigliano, C., Carfagna, M., Boso, D.P., Preziosi, L., Decuzzi, P., Schrefler, B.A.: Predicting the growth of glioblastoma multiforme spheroids using a multiphase porous media model. *Biomechanics and Modeling in Mechanobiology* **15**(5), 1215–1228 (2016). DOI 10.1007/s10237-015-0755-0
50. Maugin, G.A., Epstein, M.: Geometrical material structure of elastoplasticity. *Int. J. Plasticity* **14**(1-3), 109–115 (1998)
51. Mićunović, M.V.: *Thermomechanics of Viscoplasticity—Fundamentals and Applications*. Springer, Heidelberg, Germany (2009)
52. Mollenhauer, J., Aurich, M., Muehleman, C., Khelashvili, G., Irving, T.C.: X-ray diffraction of the molecular substructure of human articular cartilage. *Connective Tissue Research* **44**, 201–207 (2003)
53. Olsson, T., Klarbring, A.: Residual stresses in soft tissue as a consequence of growth and remodeling: application to an arterial geometry. *European Journal of Mechanics—A/Solids* **27**, 959–974 (2008)
54. Preston, S., Elżanowski, M.: Material Uniformity and the Concept of the Stress Space, chap. *Continuous Media with Microstructure*, pp. 91–101. Springer Berlin Heidelberg, Berlin, Heidelberg (2010)
55. Preziosi, L., Ambrosi, D., Verdier, C.: An elasto-visco-plastic model of cell aggregates. *J. Theor. Biol.* **262**(1), 35–47 (2010)
56. Preziosi, L., Farina, A.: On darcy’s law for growing porous media. *Int. J. Non-Linear Mech.* **37**(3), 485–491 (2002)
57. Preziosi, L., Vitale, G.: A multiphase model of tumor and tissue growth including cell adhesion and plastic reorganization. *Math. Models Methods Appl. Sci.* **21**, 1901–1932 (2011)
58. Rodriguez, E.K., Hoger, A., McCullogh, A.D.: Stress-dependent finite growth in soft elastic tissues. *Journal of Biomechanics* **27**, 455–467 (1994)
59. Sadik, S., Yavari, A.: On the origins of the idea of the multiplicative decomposition of the deformation gradient. *Mathematics and Mechanics of Solids* **22**(4), 771–772 (2017). DOI 10.1177/1081286515612280
60. Taber, L.: Biomechanics of growth, remodeling, and morphogenesis. *ASME Applied Mechanics Review* **48**(8), 487–545 (1995)
61. Tomic, A., Grillo, A., Federico, S.: Poroelastic materials reinforced by statistically oriented fibres - numerical implementation and application to articular cartilage. *IMA Journal of Applied Mathematics* **79**, 1027–1059 (2014)